ARMA MODEL BASED CLUTTER ESTIMATION AND ITS EFFECT ON CLUTTER SUPRESSION ALGORITHMS

A THESIS SUBMITTED TO
THE GRADUATE SCHOOL OF NATURAL AND APPLIED SCIENCES
OF
MIDDLE EAST TECHNICAL UNIVERSITY

BY

GÜNEŞ TANRIVERDİ

IN PARTIAL FULFILLMENT OF THE REQUIREMENTS
FOR
THE DEGREE OF MASTER OF SCIENCE
IN
ELECTRICAL & ELECTRONICS ENGINEERING

JUNE 2012

Approval of the thesis:

ARMA MODEL BASED CLUTTER ESTIMATION AND ITS EFFECT ON CLUTTER SUPRESSION ALGORITHMS

submitted by **GÜNEŞ TANRIVERDİ** in partial fulfillment of the requirements for the degree of **Master of Science in Electrical and Electronics Engineering Department, Middle East Technical University** by,

Prof. Dr. Canan Özgen
Dean, Graduate School of **Natural and Applied Sciences, METU** _____

Prof. Dr. İsmet Erkmen
Head of Department, **Electrical and Electronics Engineering, METU** _____

Prof. Dr. Seyit Sencer Koç
Supervisor, **Electrical and Electronics Engineering Dept., METU** _____

Examining Committee Members:

Prof. Dr. Yalçın Tanık _____
Electrical and Electronics Engineering Dept., METU

Prof. Dr. Seyit Sencer Koç _____
Electrical and Electronics Engineering Dept., METU

Prof. Dr. Mete Severcan _____
Electrical and Electronics Engineering Dept., METU

Assoc. Prof. Dr. Çağatay Candan _____
Electrical and Electronics Engineering Dept., METU

Dr. Ülkü Doyuran _____
Aselsan Inc.

Date: 07/06/2012

I hereby declare that all information in this document has been obtained and presented in accordance with academic rules and ethical conduct. I also declare that, as required by these rules and conduct, I have fully cited and referenced all material and results that are not original to this work.

Name, Last Name : GÜNEŞ TANRIVERDİ

Signature :

ABSTRACT

ARMA MODEL BASED CLUTTER ESTIMATION AND ITS EFFECT ON CLUTTER SUPRESSION ALGORITHMS

Tanrıverdi, Güneş

M.Sc., Department of Electrical & Electronics Engineering

Supervisor : Prof. Dr. Seyit Sencer Koç

June 2012, 103 pages

Radar signal processing techniques aim to suppress clutter to enable target detection. Many clutter suppression techniques have been developed to improve the detection performance in literature. Among these methods, the most widely known is MTI plus coherent integrator, which gives sufficient radar performance in various scenarios. However, when the correlation coefficient of clutter is small or the spectral separation between the target and clutter is small, classical approaches to clutter suppression fall short.

In this study, we consider the ARMA spectral estimation performance in sea clutter modelled by compound K-distribution through Monte Carlo simulations. The method is applied for varying conditions of clutter spikiness and auto correlation sequences (ACS) depending on the radar operation. The performance of clutter suppression using ARMA spectral estimator, which will

be called ARMA-CS in this work, is analyzed under varying ARMA model orders.

To compare the clutter suppression of ARMA-CS with that of conventional methods, we use improvement factor (IF) which is the ratio between the output Signal to Interference Ratio (SIR) and input SIR as performance measure. In all cases, the performance of ARMA-CS method is better than conventional clutter suppression methods when the correlation among clutter samples is small or the spectral separation between target and clutter is small.

Keywords: K-Distribution, Sea Clutter, Internal Clutter Motion (ICM), Autoregressive Moving Average (ARMA), Clutter Suppression, Improvement Factor

ÖZ

ARMA MODEL TABANLI KARGAŞA TAHMİNİ VE KARGAŞA BASTIRMA ALGORİTMALARINA ETKİSİ

Tanrıverdi, Güneş

Yüksek Lisans, Elektrik & Elektronik Mühendisliği Bölümü

Tez Yöneticisi : Prof. Dr. Seyit Sencer Koç

Haziran 2012, 103 sayfa

Radar sinyal işleme teknikleri hedef tespitini mümkün kılmak için kargaşa sinyalini bastırmayı hedeflemektedir. Literatürde bulunan birçok kargaşa bastırma tekniği hedef tespit performansını arttırmak için geliştirilmiştir. Bu yöntemler arasında çeşitli senaryolar altında yeterli seviyede performans sağlayan MTI ardından eşevreli entegratör en bilinen yöntemdir. Fakat kargaşa sinyalleri arasındaki korelasyon az veya hedef ile kargaşa arasındaki spektral uzaklık küçük olduğu durumda, klasik kargaşa bastırma yaklaşımları yetersiz kalmaktadır.

Bu çalışmada, Monte Carlo benzetimleri ile K-dağılımlı deniz kargaşasının ARMA spektral kestirim yöntemi ile modellenme performansı incelenmiştir. Yöntem radar çalışma ortamına bağlı olarak değişik kargaşa şekilsel yapılarına ve otokorelasyon dizilerine (ACS) için değerlendirilmiştir. Çalışma sırasında

ARMA-CS olarak adlandırılmış kargaşa bastırma amacıyla ARMA spektral kestirimini kullanan yöntemin performansı değişen ARMA model seviyelerine göre analiz edilmiştir.

ARMA-CS yönteminin klasik yöntemlere göre kargaşa bastırma performansını karşılaştırmak için ölçü olarak çıkıştaki Sinyal ile Enterferans Oranı (SIR) ile girişteki SIR seviyesinin birbirlerine oranı olarak tanımlanan iyileştirme faktörü (IF) kullanılmıştır. Kargaşa sinyalleri arasındaki korelasyon az veya hedef ile kargaşa arasındaki spektral uzaklığın küçük olduğu durumlarda ARMA-CS yöntemi klasik yöntemlere göre daha yüksek başarım sağlamaktadır.

Anahtar Kelimeler: K-Dağılımı, Deniz Kargaşası, ICM, ARMA, Kargaşa Bastırma, İyileştirme Faktörü

To My Family

ACKNOWLEDGEMENTS

I have completed my thesis with assistance of various people who helped me during my studies. I would like to take this opportunity to acknowledge their help.

Firstly, I wish to express my deepest gratitude to my supervisor Prof. Dr. Seyit Sencer Koç for his guidance, advice, criticism and insight throughout this research.

I am also grateful to ASELSAN Inc. for her opportunities and supports during the completion of this thesis.

I would like to thank to Hüseyin Emre Güven for his continuous support during this study.

Special appreciation and gratitude are also for my family for their constant care and understanding, encouragement and endless love throughout my life.

TABLE OF CONTENTS

LIST OF TABLES

TABLES

LIST OF FIGURES

FIGURES

LIST OF ABBREVIATIONS

ACS	Auto Correlation Sequence
AC	Alternating Current
AIC	Akaike Information Criterion
AICC	Akaike Information Corrected Criterion
AR	Autoregressive
ARMA	Autoregressive Moving Average
ARMA-CS	ARMA Clutter Suppressor
CDF	Cumulative Distribution Function
CNR	Clutter to Noise Ratio
CI	Coherent Integrator
DC	Direct Current
DTFT	Discrete Time Fourier Transform
FFT	Fast Fourier Transform
FIR	Finite Impulse Response
FPE	Final Prediction Error
ICM	Internal Clutter Motion
IF	Improvement Factor
MA	Moving Average
MC	Monte Carlo
MTI	Moving Target Indication
MSE	Mean Square Error

PDF	Probability Density Function
PRF	Pulse Repetition Frequency
PSD	Power Spectral Density
RCS	Radar Cross Section
RMS	Root Mean Square
SMI	Sample Matrix Inversion
SIR	Signal to Interference Ratio
SIRP	Spherically Invariant Random Process
WSS	Wide Sense Stationary
ZMNL	Zero Memory Nonlinear Transformation

CHAPTER 1

INTRODUCTION

1.1. Radar Definition and Interference Suppression

RADAR (RAdio Detection And Ranging) is a device that uses electromagnetic waves to remotely sense the position, velocity, angle and identifying characteristics of a target. Radar accomplishes this task by illuminating a volume of space with electromagnetic energy and sensing the returning echoes from environment.

In the illuminated volume, not only the target but other objects causing interference are also present. Interference is defined as unwanted radar returns from environmental or manmade sources, such as noise, jamming and clutter.

There are two sources of noise: the external noise and internal noise [1]. The external noise is received through the antenna of the radar and mainly caused by sun. The intrinsic noise which is also called thermal noise is the dominant noise component and is caused by conducting and semiconducting devices within the receiver. The noise in radar systems are modeled as a zero-mean, white, Gaussian process [1]. In literature, there are signal processing operations to increase the target signal level with respect to noise level; such as matched filtering [1].

Jammers are man-made interference sources and can be separated into active jamming (noise transmitters) and passive jamming [1]. Jamming is used to degrade the ability of radar to detect targets. There are methods to suppress jamming signals in literature, such as adaptive beam forming [1].

Clutter is defined as the electromagnetic returns caused by the environment. The source of clutter may be ground, weather or sea. It is a band-limited signal which has to be suppressed to increase the radar performance.

Clutter filtering and Doppler processing are closely related techniques that are used to suppress the clutter signals [1]. Both techniques exploit the spectral separation of target and clutter, which is mainly caused by Doppler shift of moving echoes. The conceptual difference of the clutter filtering and Doppler processing is that the former implies the time domain, whereas the latter uses frequency domain [1].

Clutter filtering; mostly known as Moving Target Indication (MTI), is a high pass filtering technique used to suppress the constant components of the signal which is caused by stationary clutter. It is mostly implemented as a first order or a second order digital filter in time domain [1]. Depending on the radar platform and operation, different types of MTI filters are observed, such as airborne MTI (AMTI), ground MTI (GMTI) and combination of both types.

Doppler processing generally implies the use of discrete Fourier transform (FFT) or some other spectral estimation techniques (correlogram, AR or ARMA… etc) to determine the spectrum of the radar return signal from a number of pulses [1]. The idea behind this technique is that the target signal and clutter signal are spectrally separated due to their Doppler shifts. Therefore, the clutter signal can be suppressed by the use of Doppler processing.

In most pulsed radar systems, the clutter filtering and Doppler processing are implemented together [1].

In order to suppress clutter, other spectral estimators can be used. By modeling the spectrum of clutter (or interference signal) with parametric spectral estimation methods (AR, MA or ARMA), the estimated spectrum can be obtained with model parameters. Modeling the spectrum with a parametric spectral estimator is equivalent to modeling the return signal as a parametric filter [1]. The clutter signal can be suppressed with the utilization of the parametric filter which is obtained by taking the inverse of parametric filter [1].

With the above idea, the ARMA spectral estimator, which requires small model order parameters than AR or MA methods for a certain signal, is used to develop a clutter suppressor, which is called as ARMA-CS, to suppress the interference signal in the thesis.

1.2. Thesis Motivation

In radar systems, many signal processing techniques have been developed to suppress the K-distributed clutter and increase the detection and estimation performance. For this purpose, the signal processing techniques mainly utilize the spectral separation between the target and clutter with Gaussian distributed clutter assumption. The performance of classical approaches fall short when the clutter distribution is changed, number of processed pulses is small, correlation among clutter samples is small or the spectral separation between the target and clutter is small.

The main motivation of the work in the thesis is to investigate the performance of clutter suppression using ARMA spectral estimator, which will be called ARMA-CS in this work, in K-distributed clutter especially when the number of processed pulses, correlation among clutter samples and spectral separation between target and clutter are small. For generation of K-distributed clutter, sea clutter model which is well developed in literature is used. The sea clutter is assumed to have a K-distribution, since its shape parameter can be used to model different scenarios and experimental results confirm its applicability [2].

The improvement factor obtained with ARMA-CS method is investigated and compared to those of the conventional techniques.

1.3. Thesis Organization

The main objectives of the thesis can be listed as follows:

- Explaining the characteristics of K-distributed sea clutter
- Analyzing the effects of antenna scanning modulation and internal clutter motion (ICM) on sea clutter
- Examining the target signal and noise models
- Investigating non-parametric and parametric spectral estimation techniques
- Determining the RMS error to estimate the spectrum of K-distributed clutter signal with ARMA method for several model orders and clutter spikiness
- Comparing the clutter suppression of ARMA-CS with that of conventional estimator with the measure of improvement factor

There are totally 6 chapters in the thesis. Chapter 1 presents the radar terminology and interference suppression concepts and outlines the work done in the thesis. Chapter 2 explains the characteristics of K-distributed sea clutter, target signal and noise models. Chapter 3 covers the non-parametric and parametric spectral estimation techniques. Chapter 4 investigates the ARMA spectral estimation performance in modeling clutter PSD for different ARMA model orders. Chapter 5 gives the comparisons of ARMA-CS and conventional methods in clutter suppression via improvement factor (IF) as a performance measure.

CHAPTER 2

BACKGROUND

2.1. Problem Statement

In this thesis, the main problem that is tried to be solved is to estimate the covariance matrix of the K-distributed clutter signal with autoregressive moving average (ARMA) spectral estimation method. Of course, the received signal is assumed to be contaminated by thermal noise. The covariance matrix estimate is then used in signal processing algorithms to suppress the clutter. For simulation purposes, K-distributed sea clutter signal and white Gaussian thermal noise, which is unavoidable in a practical radar system, are generated to see the ARMA spectral estimator performance in modeling sea clutter for different clutter parameters. The target echo is also generated to evaluate the effect of ARMA-CS method compared with several processors. For this purpose, in this chapter, first K-distributed sea clutter model, target echo model and noise signal models are introduced.

2.2. Sea Clutter

Sea clutter is defined as the unwanted and unavoidable radar returns from the sea surface. For operational marine radar systems, the performance is limited by their ability to detect targets in the presence of sea clutter environment. Therefore, radar signal processing algorithms must be optimized for the level of conditions likely to be encountered in the sea environment.

In modeling sea clutter, dynamics of sea and parameters of the radar system must be considered. The parameters affecting the measured backscatter from the sea surface are the carrier frequency, instantaneous bandwidth, antenna pattern and beam-width, thermal noise, pulse repetition frequency (PRF), polarization, angle of incidence and the range of the radar to the center of clutter. On the other hand, the dynamics of sea affecting the measured backscatter from the sea surface are the sea state, the speed, duration and direction of the wind, sea wave speed, the fetch and sea swell direction [2].

In the coarse level, sea clutter is characterized by the sea waves and sea state. Two kinds of waves are mostly encountered in the sea environment: the capillary waves and the gravity waves (swells). The capillary waves are mainly generated by the wind. This kind of waves is small in amplitude and very large in number, having short wavelengths (less than 2 centimeters). These waves have almost random motion and can be observed in the still weather. Moreover, the capillary waves do not have much impact energy [3].

The capillary waves are superimposed on the gravity waves; which are accumulated by gravitational forces. At the beginning, these waves are generated by some meteorological phenomena (wind, storm… etc), but their properties are eventually determined by the sea state. Gravity waves have larger amplitudes and larger wavelength (more than 2 cm) than capillary waves. They are the main energy carrying factor of the sea clutter [3].

The capillary waves superimposed on gravity waves and their interaction with the electromagnetic waves is illustrated in Figure 2-1.

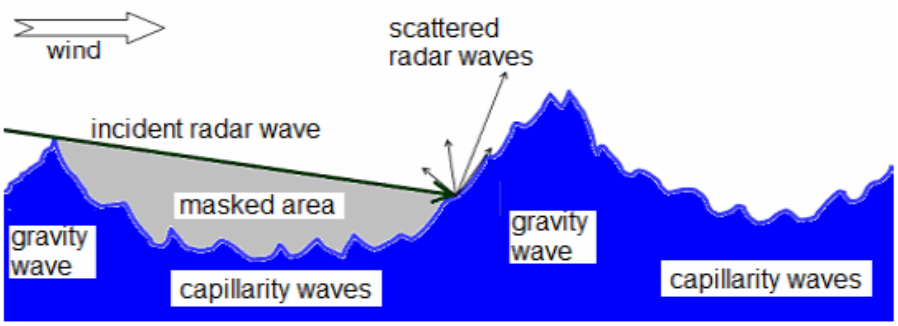

Figure 2-1: The Phenomenological Model of Sea Surface

2.2.1. Characteristics of Sea Clutter

In this section, sea clutter characteristics and modeling sea clutter are investigated. For this purpose, amplitude characteristics and correlation properties of sea clutter are first covered; then, numerical generation of sea clutter is discussed.

2.2.1.1. Amplitude Characteristics

Sea clutter returns are spatial and temporal stochastic processes which exhibit noise-like behavior [2]. Therefore, the characterization of amplitude behavior of sea clutter has utmost importance in optimum radar performance analysis.

The experimental data show that although sea clutter obeys central limit theorem, for high resolution and low grazing angle radars, the amplitude variances are significantly larger than those predicted by Rayleigh Probability Density Function [2]. Hence, more realistic models that agree with the experimental data are developed. In thesis, K-distribution is used to model the amplitude statistics of sea clutter returns. However, for the sake of

completeness the distribution models used to generate sea clutter amplitude statistics in literature are given along with their cumulative distribution function (CDF) and probability density function (PDF) in Table 2-1 [2]. In this table, α is the amplitude return of the signal and is defined in the range $0 \le \alpha \le \infty$.

Table 2-1: Models for Sea Clutter Amplitude Distributions

Model	CDF	PDF
Rayleigh	$\mathrm{F_R}(\alpha) = 1 - \exp\left[-\left(\frac{\alpha}{\omega}\right)^2\right]$	$f_R(\alpha) = \frac{2\alpha}{\omega^2}\exp\left[-\left(\frac{\alpha}{\omega}\right)^2\right]$
Log-Normal	$F_L(\alpha) = \Phi\left(\frac{\ln\alpha - \mu}{\sigma}\right)$	$f_L(\alpha) = \frac{1}{\sqrt{2\pi}\sigma\alpha}\exp\left[-\frac{(\ln\alpha - \mu)^2}{2\sigma^2}\right]$
Weibull	$F_W(\alpha) = 1 - \exp\left[-\exp\left(\frac{\alpha}{\omega}\right)^\gamma\right]$	$f_W(\alpha) = \frac{\gamma}{\omega}\left(\frac{\alpha}{\omega}\right)^{\gamma-1}\exp\left[-\left(\frac{\alpha}{\omega}\right)^\gamma\right]$
K-Distribution	$F_K(\alpha) = 1 - \frac{2}{\Gamma(\nu)}\left(\frac{c\alpha}{2}\right)^\nu K_\nu(ca)$	$f_K(\alpha) = \frac{2c}{\Gamma(\nu)}\left(\frac{c\alpha}{2}\right)^\nu K_{\nu-1}(ca)$

In Table 2-1, ω is the scale parameter for Rayleigh and Weibull distributions; $\Gamma(z)$ is the Gamma function; $\ln(\alpha)$ is Normally distributed with mean μ and variance σ^2 for Log-Normal distribution; γ is the shape parameter for Weibull distribution; c is the scale parameter and ν is the shape parameter for K-Distribution; $K_\nu(z)$ is the modified Bessel function of the second kind of order ν and $\Phi(z) = \int_{-\infty}^{z}\frac{1}{\sqrt{2\pi}}\exp\left(-\frac{t^2}{2}\right)dt$.

As mentioned before, among these amplitude distribution models given in Table 2-1, K-Distribution is a good description of the sea clutter amplitude statistics and is the most promising model of sea clutter. The reason for this behavior is that log-normal and Weibull amplitude distributions do not include the spatial and temporal correlation in the sea clutter returns [2]. Hence, K-Distribution for the sea clutter model is investigated in more detail in the following sub-sections.

2.2.1.1.1. K-Distributed Sea Clutter Model

The compound K-Distributed amplitude distribution for sea clutter returns was first proposed by Ward in 1981 [4]. The sea clutter amplitude returns are represented by two components; the slowly varying component (texture) and the fast varying component (speckle) [2].

The first component, which is the slowly varying component, is an underlying mean level in generalized Chi-Distribution. It is caused by the gravity waves on the sea surface and has a long temporal decorrelation period (order of seconds). The slowly varying component exhibits spatial correlation which is coupled to the temporal correlation [2].

A model probability density function of slowly varying component is given in equation (2.1).

$$f(y) = \frac{2d^{2\nu} y^{2\nu-1}}{\Gamma(\nu)} \exp\left(-d^2 y^2\right). \tag{2.1}$$

Here, $\Gamma(\nu)$ is the Gamma function, ν is the shape parameter and d is a scale parameter such that $d^2 = \frac{\nu}{E(y^2)}$ where $E(y^2)$ is the mean clutter power.

The fast varying component, which is also termed the 'speckle' component, has Rayleigh distributed amplitude fluctuations. It is mainly caused by the capillary waves on the sea surface and has a fast decorrelation time (order of milliseconds). Due to fast decorrelation time, the speckle component can be considered as noise-like clutter and has spatial correlation corresponding in pulse length. Unlike the slowly varying component of sea clutter returns, speckle component can be decorrelated by frequency agility [2].

A model probability density function of speckle component is given in equation (2.2).

$$f(\alpha \mid y) = \frac{\alpha\pi}{2y^2} \exp\left(-\frac{\alpha^2\pi}{4y^2}\right). \tag{2.2}$$

Here, y is the underlying average level determined by (2.1).

Overall amplitude distribution of sea clutter returns is K-Distributed and is given in (2.3).

$$f_K(\alpha) = \int_0^\infty f(\alpha \mid y) f(y) dy = \frac{2c}{\Gamma(\nu)} \left(\frac{c\alpha}{2}\right)^\nu K_{\nu-1}(c\alpha). \tag{2.3}$$

Here, $K_\nu(z)$ is a ν^{th} order modified Bessel function of second kind and $c = \sqrt{\pi} d$ is a scale parameter.

The spikiness of sea clutter returns are determined by the shape parameter ν, the value of which falls in the range $0 \le \nu < \infty$. However, in practice, ν can be varied between 0.1, corresponding to very spiky amplitude data and 20 corresponding to Rayleigh distributed amplitude returns [2].

The power characteristic of return signal is determined by the scale parameter c. When the scale parameter becomes smaller in value, the sea clutter returns become more powerful [2]. The scale parameter can be estimated by (2.4).

$$c^2 = \frac{4\nu}{P_C}. \tag{2.4}$$

where P_C is the mean clutter power value which is determined by the radar parameters, radar-clutter geometry and mean clutter reflectivity value σ_0. The mean clutter reflectivity value is determined by Sittrop (SIT), the Georgia Institute of Technology (GIT), the Technology Service Corporation (TSC), and the Dockery (HYB) models [2].

2.2.1.1.2. Empirical Models for Shape Parameter of K-Distribution

The shape parameter ν of K-distributed sea clutter is a very crucial since it gives information about the amplitude statistics of the returns (the spikiness) and some of the correlation properties among clutter samples. For this reason, empirical formulas are developed so as to estimate the shape parameter [2]. Although the formulas for the prediction of the shape parameter are developed in X-band, they still have valuable information for amplitude statistics. The model is illustrated in (2.5)

$$\log(\nu) = \frac{2}{3}\log(\Phi) + \frac{5}{8}\log(l) + \delta - k. \tag{2.5}$$

Here ν is the shape parameter, l is the cross-range resolution, Φ is the grazing angle in degrees ($0.1^0 < \Phi < 10^0$), δ is the aspect dependency where;

$\delta = -1/3$ for up or down swell directions,

$\delta = 1/3$ for cross-swell directions and,

$\delta = 0$ for no swell conditions and intermediate swell directions.

k is a parameter that accounts for the polarization effects with $k = 1$ for vertical polarization and $k = 1.7$ for horizontal polarization.

This empirical model was proposed by Ward [5]. In this model, the shape parameter is related to grazing angle, cross-range resolution, the sea swell direction and polarization. Since the model was derived from the experimental data obtained by a radar having 30 ns pulse length, the model does not take the range resolution into account.

Another empirical model which can be used for any radar range resolution is developed by Ryan and Johnson [6]. This model is a modified version of (2.5) and the pulse length variable τ_{PULSE} is included into the formula as shown below:

$$\log(\nu) = \frac{2}{3}\log(\Phi) + \frac{5}{8}\log(l) + \delta - k + \log\left(\frac{\tau_{PULSE}}{30}\right)\log\left(\frac{50}{\Phi}\right)\log(5.5\Phi)^{0.8} \quad . \qquad (2.6)$$

The parameters in (2.6) are the same as those in (2.5).

2.2.1.2. Correlation Properties of Sea Clutter

As mentioned earlier, sea clutter returns contain both temporal and spatial correlation properties due to the structure of sea waves. Therefore, in the following sub-sections, a full treatment of the temporal and spatial correlation properties of K-distributed sea clutter model is given.

2.2.1.2.1. Temporal Correlation

Sea clutter signal coming from a single resolution cell are band limited and generally not independent in time. This correlation property within a resolution cell is defined as temporal correlation of sea clutter.

The composite model for sea clutter can be used to describe structure of temporal correlation within resolution cells. In a short time period, Rayleigh-distributed reflections are always observed within a resolution cell (speckle component) which has a Chi-distributed underlying mean level [2].

Although the speckle component of sea clutter returns has a short temporal decorrelation time (a few milliseconds), underlying mean level has a long decorrelation time [2]. Hence, the temporal decorrelation function has a fast drop-off which is followed by a slower decay [2,7].

For operational situations, the radar coherent processing intervals are very short such that the return clutter signal strength from a resolution cell remains constant. As a result, the temporal fluctuations within radar dwell time are neglected and the correlation property of sea clutter return is dictated by rapidly varying component [2].

Therefore, when the sample of time series from a resolution cell is removed before correlation is performed, the autocorrelation function of speckle component can be found [2]:

$$ACF_k = \frac{\sum_{n=0}^{N-1} x_n x_{n+k}^*}{\sum_{n=0}^{N-1} x_n x_n^*}. \tag{2.7}$$

where $(\cdot)^*$ denotes the complex conjugate; x_n is the complex received signal;

$$x_n = a_n \exp(j\theta_n). \tag{2.8}$$

$$a_n = \sqrt{x_{in}^2 + x_{qn}^2}\ . \tag{2.9}$$

$$\theta_n = \arctan\left(\frac{x_{in}}{x_{qn}}\right). \tag{2.10}$$

Here, a_n and θ_n are the envelope magnitude and phase of the quadrature components, respectively, and subscripts i and q denote the in-phase and out-of-phase quadrature components.

It is known that when the autocorrelation function is real and even, the spectrum would become symmetrical around the zero Doppler (y-axis in rectangular coordinate system) [8]. If there is a Doppler shift in the spectrum, the autocorrelation function is obtained by multiplying the real function from zero Doppler shift case by a complex exponential $\exp(\pm j\omega_d T)$ where ω_d is the angular Doppler frequency and T is the time lag [2]. Hence, for a symmetrical sea clutter spectrum which is a Gaussian function the spectral width and Doppler shift can be determined from autocorrelation function [2].

2.2.1.2.2. Spatial Correlation

The spatial correlation of sea clutter returns is defined as cross correlation between two patches of sea in radial dimension when the temporal decorrelation is negligibly small [2].

The spatial correlation of sea clutter returns are mainly related to the surface profile of the sea. Over the sea surface, the microwave signals are primarily scattered by capillary waves (speckle), but the gravity waves which are the main source of spatial correlation causes variations in the mean power scattered from a given patch (modulating process) [2]. It is logical to reason that the degree of correlation of the modulating process between resolution cells depends on the spatial correlation of the sea surface and the decorrelation

distance of the process is the same with the decorrelation distance of the sea [2].

In the compound model of sea clutter, the speckle component is assumed to be entirely uncorrelated from one range cell to the next [2].

Hence, the spatial correlation function is defined as the summation of a spike at the origin and a scaled version of the spatial autocorrelation function of the modulating process. For analysis and modeling purposes, spatial autocorrelation of mean clutter reflectivity rather than spatial autocorrelation of modulating component is preferred [2]. Mean clutter reflectivity can be expressed as follows:

$$\tau_i = 4\frac{y_i^2}{\pi} = \bar{a}_i^2 . \tag{2.11}$$

where τ_i is the average clutter reflectivity, y_i is local mean level of the clutter and $\bar{a}_i^2$ is the squared amplitude of the reflected signal averaged over successive pulses from i^{th} range cell.

2.2.1.3. Simulation of Sea Clutter Returns

As mentioned earlier, sea clutter has a non-Gaussian distribution, and generating correlated non-Gaussian random variables requires jointly specified probability density function (PDF) and covariance matrix. In literature, non-Gaussian clutter samples can be generated using zero memory nonlinear (ZMNL) transformations applied on a Gaussian sequence or applying the theory of spherically invariant random process (SIRP) [2].

In this thesis, SIRP technique is used to model sea clutter returns since the mean vector, a covariance matrix and a characteristic first-order PDF of a vector generated by theory of SIRP are uniquely determined [2].

In SIRP approach, the sea clutter amplitude returns are modeled by a multiplication of two independent processes;

$$x(t) = y(t)v(t) \ . \tag{2.12}$$

where $x(t)$ is the amplitude return of sea clutter, $v(t)$ is a zero mean complex correlated Gaussian process and $y(t)$ is a real, non-negative, stationary non-Gaussian process [2]. In (2.12), $y(t)$ is the modulating component and has a longer decorrelation time than $v(t)$ which is generated by complex white Gaussian process filtered by a linear system [2]. By this way, the amplitude and correlation properties of sea clutter returns are independently controlled by first order PDF of $f(y)$ of the modulating process $y(t)$ and by the Gaussian process $v(t)$, respectively.

In [9], $f(y)$ is given for K-distributed random process as follows (generalized Chi-PDF);

$$f(y) = \frac{2v^{v}}{\Gamma(v)} y^{2v-1} \exp\left(-vy^{2}\right). \tag{2.13}$$

Finally, when decorrelation time of modulating component $y(t)$ is long compared to time periods, the sea clutter returns are modeled by the product of a Gaussian process $v(t)$ and a modulating random variate y rather than a modulating random process $y(t)$: $x(t) = yv(t)$ which is the SIRP [2].

The complex multivariate PDF of the SIRP $x(k)$ is as follows [2];

$$f_{x}(\bar{x}) = (2\pi)^{-N} |M|^{-1/2} \int_{0}^{\infty} y^{-2N} \exp\left[\frac{-(\bar{x}-\bar{m})^{T} M^{-1} (\bar{x}-\bar{m})}{2y^{2}}\right] f(y) dy \ . \tag{2.14}$$

where $\bar{x}$ is a 2N dimensional vector whose elements are N samples from in phase and quadrature components, $\overline{m}$ is the mean vector of $\bar{x}$ and M is the covariance matrix of $\bar{x}$.

Because of the structure of $\bar{x}$, the covariance matrix M has the following form [2];

$$M = \begin{bmatrix} M_{CC} & M_{CS} \\ M_{SC} & M_{SS} \end{bmatrix}. \tag{2.15}$$

Here, M_{CC} and M_{SS} are covariance matrices of in-phase and quadrature components; M_{CS} and M_{SC} are cross-covariance matrices.

In [10], the conditions for a SIRP satisfied are given in detail and sea clutter returns obey these conditions.

Sea clutter returns are generated by following a list of steps. With this method, a complex N-dimensional vector whose modulating component is assumed to be constant in a range cell but varies from cell to cell according to the PDF of the modulating component is obtained [2].

i. The modulating component y is generated from equation (2.13);

ii. An N-dimensional complex zero-mean white Gaussian random vector W which has identity covariance matrix is generated;

iii. N-dimensional spherically invariant complex random vector (SIRV) V with the desired covariance matrix is generated using the linear transformation

$$V = GW. \tag{2.16}$$

where

$$G = ED^{1/2}. \tag{2.17}$$

Here, E is the matrix of normalized eigenvectors of covariance matrix M and D is the diagonal matrix of eigenvalues of M.

iv. The envelope of N-dimensional vector V is the Rayleigh distributed N-dimensional vector U and the phase of N-dimensional vector V is uniformly distributed. Finally, N-dimensional K-distributed amplitude return of sea clutter A and N-dimensional complex sea clutter return X are generated as:

$$A = y|V|. \tag{2.18}$$

$$X = yV. \tag{2.19}$$

2.2.2. Clutter Autocorrelation Model

In this section, the clutter covariance matrix is considered. The clutter covariance matrix determines the power spectral density of the clutter; and hence it also determines the performances of different processors. The clutter covariance matrix is mainly determined by two factors: the antenna scanning modulation, and the internal clutter motion. Depending on the parameters of the radar, either of the two factors may be the dominant cause of clutter covariance matrix. However, in some cases, both of the factors affect the clutter return signal received by the radar.

2.2.2.1. Antenna Scanning Modulation

In a mechanically scanned radar system, the decorrelation of clutter signal is mainly caused by the angular motion of the antenna. Due to the rotation, the

radar receives echoes from different patches of the scattering surface during a coherent integration interval (CPI), which causes a loss of correlation.

By approximating a two way antenna pattern as a Gaussian function, which is mostly valid for 3-dB beam-width, the effects of antenna scanning can be analyzed. In (2.19), the two-way Gaussian pattern is given.

$$G(\theta) = G_0 \exp\left(-\theta^2 / 2\sigma_{\theta 2}^2\right). \tag{2.19}$$

where $\sigma_{\theta 2}$ is the equivalent two-way standard deviation of the antenna power pattern (radians) and G_0 is the on-axis antenna power gain factor. As the antenna scans the patch of reflectors, the voltage of the echo signal from elemental reflector would have a Gaussian function. The time-variation of voltage signal from each individual elemental scatterer can be written as:

$$E(t) = K \exp\left(-t^2 / 2\sigma^2\right). \tag{2.20}$$

where σ may be termed the "standard deviation" of the time function and K is a scale factor. σ can be written as

$$\sigma = \frac{\sqrt{2}\sigma_{\theta 2}}{\alpha}. \tag{2.21}$$

where α is the rotation rate of the antenna in rad/sec.

The echo received from the clutter is a combination of all individual scattered signals, which is deterministic except for their random scale factors, K. These scattered signals are superimposed since each have the same form. Hence, the

resulting clutter echo can be considered as a random process with the same time variation. The autocorrelation of clutter is the

$$R_c(t) = A\exp\left(-t^2/2\sigma^2\right). \tag{2.22}$$

The power spectral density of the clutter is obtained by taking the squared magnitude of the Fourier transform of (2.22), which is

$$S_c(\omega) = C_0\exp\left(-\omega^2/2\sigma_\omega^2\right). \tag{2.23}$$

where σ_ω is the standard deviation of the spectrum in rad/sec, and ω is the radian frequency variable. We can relate σ_ω (rad/sec) to physical parameters of the radar as,

$$\sigma_\omega = \frac{\alpha}{2\sigma_{\theta 2}}. \tag{2.24}$$

The standard deviation of the antenna pattern $\sigma_{\theta 2}$ may be expressed in terms of the two-way half-power azimuth beam-width θ_{B2}, which for a Gaussian pattern is:

$$\theta_{B2} = \sqrt{8\ln 2}\,\sigma_{\theta 2}. \tag{2.25}$$

When the transmit and receive antennas are identical, the two-way half-power azimuth beam-width θ_{B2}, can be expressed in terms of the transmit antenna half power azimuth beam-width θ_B as

$$\theta_{B2} = \frac{\theta_B}{\sqrt{2}}. \tag{2.26}$$

Finally, with these results the spectrum width σ_s induced by antenna scanning (in Hz) can be determined as

$$\sigma_s = \frac{\sqrt{8\ln 2}}{4\pi}\frac{\alpha}{\theta_{B2}} = \frac{\sqrt{\ln 2}}{\pi}\frac{\alpha}{\theta_B}. \tag{2.26}$$

The resulting covariance function of clutter will have the following structure;

$$\mathbf{M} = \begin{bmatrix} 1 & e^{-1/2\sigma_s^2} & e^{-4/2\sigma_s^2} & \cdots & e^{-(n-1)^2/2\sigma_s^2} \\ e^{-1/2\sigma_s^2} & 1 & e^{-1/2\sigma_s^2} & \cdots & e^{-(n-2)^2/2\sigma_s^2} \\ e^{-4/2\sigma_s^2} & e^{-1/2\sigma_s^2} & 1 & \cdots & e^{-(n-3)^2/2\sigma_s^2} \\ \vdots & \vdots & \vdots & \ddots & \vdots \\ e^{-(n-1)^2/2\sigma_s^2} & e^{-(n-2)^2/2\sigma_s^2} & e^{-(n-3)^2/2\sigma_s^2} & \cdots & 1 \end{bmatrix}. \tag{2.27}$$

2.2.2.2. Internal Clutter Motion

Clutter is typically modeled as a delta function at zero Doppler velocity. However, because of motions of objects (e.g., trees, vegetation, etc) within a clutter cell, the clutter would have a non-zero bandwidth [11]. This phenomenon is termed internal clutter motion (ICM) and results in pulse to pulse decorrelation of clutter returns.

For land clutter, mathematical model for the spectrum of moving clutter that fits well to the experimental data is given by

$$P_c(f) = \frac{r}{r+1}\delta(f) + \frac{1}{r+1}\frac{\beta\lambda}{4}e^{-\frac{\beta\lambda}{2}|f|} \quad . \tag{2.28}$$

In this equation f is the clutter Doppler shift (in Hz), λ is the radar wavelength, $\delta(.)$ is the Dirac delta function and β is the shape parameter which is invariant with carrier frequency and which depends on wind conditions. A table of values for β can be found in [12]. The spectrum given in (2.28) has a stationary (DC) term plus a noise (AC) term having exponential distribution. In (2.28), the spectrum is normalized so that

$$\int_{-\infty}^{\infty} P_c(f)df = 1. \tag{2.29}$$

The ratio r between the DC and AC components of the ground scatter was shown to be a function of the carrier frequency and wind speed [11];

$$10\log r = -15.5\log w - 12.1\log f_c + 63.2. \tag{2.30}$$

where w is the wind speed in miles per hour (mph), f_c is the carrier frequency in MHz.

By taking the inverse Fourier transform we can get the correlation function

$$r_c(\tau) = \frac{r}{r+1} + \frac{r}{r+1}\frac{(\beta\lambda)^2}{(\beta\lambda)^2 + (4\pi\tau)^2}. \tag{2.31}$$

In literature, the power spectral density (PSD) of internal clutter motion (ICM) shows an exponential decay of the spectral shapes [12]. In this thesis, auto

correlation function (ACF) resulted from ICM is exponential. Therefore, the resulting covariance function of clutter will have the following structure:

$$\mathbf{M} = \begin{bmatrix} 1 & \rho & \rho^2 & \cdots & \rho^{n-1} \\ \rho & 1 & \rho & \cdots & \rho^{n-2} \\ \rho^2 & \rho & 1 & \cdots & \rho^{n-3} \\ \vdots & \vdots & \vdots & \ddots & \vdots \\ \rho^{n-1} & \rho^{n-2} & \rho^{n-3} & \cdots & 1 \end{bmatrix}. \tag{2.32}$$

where ρ is the correlation coefficient.

The ICM is effective in clutter echo when the radar is not rotating or when ICM is dominant over antenna scanning modulation. In this thesis, it is assumed that the internal clutter motion (ICM) of sea clutter is caused by winds; hence, sea clutter echo would have an exponential covariance structure like land clutter.

2.2.2.3. Effect of Internal Clutter Motion on the Clutter Covariance

When both the antenna scanning modulation and internal clutter motion are effective in clutter returns, the covariance matrix would be tapered. That is, the decorrelation effect of ICM results in an increase in the rank of clutter covariance matrix caused by antenna scanning modulation [11].

Since ICM is a temporal decorrelation and has an autocorrelation function, this decorrelation can be modeled as a covariance matrix taper in temporal covariance matrix caused by antenna scanning modulation.

$$T_{ik} = r_c((i-k)T_P). \tag{2.33}$$

Here in (2.33), T_{ij} is the $ij-th$ entry of temporal covariance matrix and T_p is the pulse repetition interval.

Therefore, covariance matrix for the clutter echo with internal clutter motion is obtained from the Hadamard product of R_C, which is the covariance matrix caused by antenna scanning modulation, with T matrix for one antenna system [11]:

$$R = R_C \circ T . \tag{2.34}$$

2.3. Target Echo Model

A model for the target signal is required to calculate the improvement factor of different processors and ARMA-CS processor.

In this section, firstly general information about the target signal distributions is given. Afterwards, the algorithm to generate target signals is described.

2.3.1. Complex Target Distributions

When an electromagnetic wave is incident upon a scattering object (or a target), some of the incident wave energy is absorbed by the object, and the rest is scattered in various directions. In fact, some of the incident energy is scattered back towards the radar. It can be assumed that the target collects all of the energy on the area σ square meter and reradiates it isotropically [1]. The quantity σ is called radar cross section (RCS) and it is a measure of the energy reradiated from the target.

RCS is a measure of the reflectivity of a radar target. The notation used for RCS is RCS σ and evaluated from:

$$\sigma = \frac{P}{Q}. \tag{2.35}$$

where P is the power scattered back towards the radar and Q is total power incident on the target.

The RCS of simple geometric shapes can be determined easily by electromagnetic calculations. However, due to complex shapes of real radar targets (aircrafts, ships, etc.) it is not easy to determine the RCS by using electromagnetic solutions. The most common procedure is to break the complex target into simple component parts and combine the determined RCS values accordingly. This approach is mainly used to determine the mean RCS over an aspect angle of the target [13]. Since in an operational situation, the aspect angle of a target to the radar is unknown, RCS is best described by statistical models.

In this thesis, Marcum (or Swerling 0) target model is used in simulations. However, for the sake of completeness, the models that are used in literature used for target statistics are given in Table 2-2 [13]. Moreover, in the following sub-sections, brief information about the target statistical models are also given.

Table 2-2: Statistical Models of Target Radar Cross Sections

Model	Density Function of RCS	Applicability
Marcum	*One Possible Value. (Deterministic)*	Perfectly steady reflector
Chi-square of degree *2m*	$\frac{m}{\Gamma(m)\bar{x}}\left[\frac{mx}{\bar{x}}\right]^{m-1}\exp\left[-\frac{mx}{\bar{x}}\right].$	The distribution encompasses a class of target distributions. Degree becomes higher as coherent component of target becomes greater [1].
Swerling cases 1 and 2	$\frac{1}{\bar{x}}\exp\left(-\frac{x}{\bar{x}}\right)$ **for** $x \geq 0$.	Random scatterers, no single one is dominant. Applies to complex targets having numerous scatterers.
Swerling cases 3 and 4	$\frac{4}{\bar{x}^2}\exp\left(-\frac{2x}{\bar{x}}\right)$ **for** $x \geq 0$.	Random scatterers, one of which is dominant. Applies to complex targets having numerous scatterers.

Table 2-3: continued

Rice (power)	$\frac{1}{\bar{x}}\left(1+a^2\exp\left[-a^2-\frac{x}{\bar{x}}\left(1+a^2\right)\right]\cdot j_0\left[2ia\sqrt{1+a^2\left(x\sqrt{x}\right)}\right]\right)$ **for** $x \geq 0$.	One large reflector and an assembly of small reflectors. a^2 is the ratio of RCS of the large to the sum of the rest.
Log-Normal	$\frac{1}{xs\sqrt{2\pi}}\exp\left(-\frac{\left(\ln x-\ln\bar{x}\right)^2}{2s^2}\right)$ **for** $x \geq 0$.	Found to apply to many targets which have large mean-to-median ratios.

In Table 2-2, x is the RCS, $2m$ is the degree of freedom, $\bar{x}$ is mean RCS, a^2 is ratio of RCS of large reflection to the sum of the small, J_0 is the modified Bessel function, i is $\sqrt{-1}$, s is standard deviation of $\ln x$, $\ln\bar{x}$ is mean distribution with $\ln x$ as the variable and $\Gamma(m)$ is gamma function with argument m.

In the subsections of this section, the applicability of these models is described [13].

2.3.1.1. Marcum Model

In Marcum model, the target signal is assumed to have no fluctuation in time. However, this is not a realistic situation for radars and is only analyzed to see the detection performance of a receiver.

2.3.1.2. Chi Square Distribution of Degree 2M

Large class of targets can be modeled in chi-square distribution. In Table 2-2, the distribution given for chi-square model is written for $2m$ degrees of

freedom. It is known that as m goes to infinity, the RCS fluctuations of target returns become more constrained and steady-target case is observed.

2.3.1.3. Swerling Cases 1 and 3

In Swerling 1 and 2 models, the target is assumed to be compose of many randomly distributed scatterers. These are often referred to as Rayleigh or exponential distributions in literature.

The difference of the Swerling 1 and Swerling 2 RCS models is the correlation of signals during radar pulses. In Swerling 1, the statistics apply when the target signals are correlated within a pulse group; however, in case 2, the RCS pulse samples are independent on a pulse-to-pulse basis. In fact, due to narrow Doppler spectra of radar pulses, the Swerling 1 assumption is valid for most of the radar targets, unless the radar uses frequency diversity in pulse-to-pulse basis. In the latter case, Swerling 2 target RCS assumption is valid.

2.3.1.4. Swerling Cases 2 and 4

Swerling 3 and 4 cases are the approximation to the case of many small scatters and one dominant scatterer. When there is pulse-to-pulse independence case 4 statistics is used; when scan-to-scan independence (dependence among several pulses) exists, case 2 statistics is used.

2.3.1.5. Rice Distribution

Rice distribution is used to model the RCS returns of small scatterers including a large reflector whose return is significant compared to the sum of all other small reflectors. In Table 2-2, the parameter a^2 is the ratio of the power from the large scatterers to the power of the rest. When a^2 converges to ∞, steady target reflection occurs; when it converges to 0 , the distribution becomes Rayleigh.

2.3.1.6. Log-Normal Distribution

Some of the target RCS distributions do not conform to any chi-square member. Some of the targets; such as satellites, missiles, ships, exhibit large values of RCS far more frequently than any other chi-square class. The RCS distributions of such targets are modeled as log-normal density functions which arise when the logarithm of a variate is normally-distributed. By using log-normal distribution which has high tails of density function, large specular returns of the class of targets can be modeled.

2.3.2. Target Signal Generation Algorithm

Marcum, Swerling 1 and 2 target signals are generated by following a list of steps. In the simulations two assumptions are accepted. Firstly, it is assumed that any target is contained in one range cell. Secondly, targets are assumed to have constant velocity (constant Doppler phase).

i. The Doppler shift is determined according to target velocity;

$$f_D = \frac{2V_R}{\lambda}. \tag{2.36}$$

where V_R denotes the radial velocity between radar and the target and λ is the wavelength of the radar signal.

ii. The target Doppler shift vector, P, is written for number of pulses in a coherent integration interval;

$$P = \begin{bmatrix} \exp(j2\pi f_D T_0) \\ \exp(j2\pi f_D T_1) \\ \vdots \\ \exp(j2\pi f_D T_{N-1}) \end{bmatrix}. \tag{2.37}$$

where T_k denotes the pulse repetition interval (PRI).

iii. Temporal correlation of target signal is adjusted by the parameter ρ. For Marcum ρ is 1, for Swerling 1 targets, ρ is close to 1, and for Swerling 2 targets, ρ is 0.

iv. The target signal covariance matrix, M, is formed using correlation coefficient;

$$\mathbf{M} = \begin{bmatrix} 1 & \rho & \rho^2 & \cdots & \rho^{N-1} \\ \rho & 1 & \rho & \cdots & \rho^{N-2} \\ \rho^2 & \rho & 1 & \cdots & \rho^{N-3} \\ \vdots & \vdots & \vdots & \ddots & \vdots \\ \rho^{N-1} & \rho^{N-2} & \rho^{N-3} & \cdots & 1 \end{bmatrix}. \tag{2.38}$$

v. Doppler shift is added into the covariance matrix of target signal;

$$M_T = M \circ (PP^H). \tag{2.39}$$

where M_T is the target signal covariance matrix with Doppler shift, , and $\circ$ denotes element wise multiplication (Hadamard product).

vi. A N-dimensional complex zero-mean white Gaussian random vector w which has identity covariance matrix is generated;

vii. N-dimensional complex target signal vector x with the desired covariance matrix is generated using the linear transformation

$$x = Gw. \tag{2.40}$$

where

$$G = ED^{1/2}. \tag{2.41}$$

Here, E is the matrix of normalized eigenvectors of covariance matrix M_T and D is the diagonal matrix of eigenvalues of M_T.

viii. Finally, the x is multiplied with the square root of target signal power which is obtained from the target RCS.

2.4. Noise Model

The thermal noise in the system is assumed to be independent and identically distributed (i.i.d.) complex white Gaussian random vector.

The noise signal with length N in the system can be written by the following equations;

$$n = n_I + jn_Q . \tag{2.42}$$

$$E\{nn^H\} = \sigma_n^2 I_{NxN} . \tag{2.43}$$

Here, n is a complex noise vector with length N, n_I which is a zero-mean Gaussian random vector is the in-phase component of complex noise signal, n_Q which is a zero-mean Gaussian random vector is the quadrature component of complex noise signal, σ_n^2 is the noise variance and I_{NxN} is an identity matrix of size NxN.

CHAPTER 3

SPECTRAL ESTIMATION CONCEPTS

3.1. Purpose of Spectral Estimation

In radars, together with the thermal noise, clutter signals are the interference signal that limits the target detection and estimation performance. In spectral estimation problem, total power distribution over frequency of a signal is estimated from finite set of stationary data [14]. Spectral estimation techniques can be applied on radar signals in order to estimate clutter spectrum which is required to suppress the clutter returns. A good estimate of clutter spectrum can improve the radar performance substantially.

3.2. Spectral Estimation

The signals in radar applications have random nature, whose future values cannot be determined exactly. At this point, the random signals are assumed to be Wide Sense Stationary (WSS) which means that 1^{st} and 2^{nd} moments of the signal do not change in time (or in space as the case may be). Moreover, to estimate the autocorrelation function of the clutter random process, the assumption that it is ergodic is made to permit the substitution of time averages by ensemble averages.

In radar applications, the discrete-time signals $\{x(t); t = 0,\pm1,\pm2,\ldots\}$ (clutter signal, noise signal, target signal…etc) are random variables which are typically zero mean. The covariance function (autocovariance sequence) of $x(t)$ is defined as;

$$r(k) = E\{x(t)x^*(t-k)\}. \tag{3.1}$$

The first definition of Power Spectral Density of a random sequence is the DTFT of the covariance sequence given by,

$$\varphi(\omega) = \sum_{k=-\infty}^{\infty} r(k)e^{-j\omega k}. \tag{3.2}$$

The inverse transform, which recovers $r(k)$ from given $\varphi(\omega)$ is;

$$r(k) = \frac{1}{2\pi}\int_{-\pi}^{\pi} \varphi(\omega)e^{j\omega k}\,d\omega. \tag{3.3}$$

From equation (3.1), it is seen that for $k = 0$, $r(0) = E\{|x(t)|^2\}$ which is the average signal power over frequencies is determined. This proves that $\varphi(\omega)$ can indeed be named as PSD.

The second definition of Power Spectral Density $\varphi(\omega)$ is as follows;

$$\varphi(\omega) = \lim_{N\to\infty} E\left\{\frac{1}{N}\left|\sum_{t=1}^{N} x(t)e^{-j\omega t}\right|^2\right\}. \tag{3.4}$$

The second PSD definition is equivalent to the first assumption under the mild assumption that the covariance sequence is $r(k)$ decays sufficiently rapidly that [14]

$$\lim_{N\to\infty}\frac{1}{N}\sum_{k=-N}^{N}\left|kr(k)\right|=0. \tag{3.5}$$

As stated earlier, in spectral estimation the main problem is finite amount of data available. With this finite data, it is desirable to obtain a good estimate $\hat{\varphi}(\omega)$ to $\varphi(\omega)$. The method used for this purpose can be classified as:

i. Non-parametric methods
ii. Parametric methods

3.2.1. Non-Parametric Spectral Estimation

In this thesis, parametric spectral estimation techniques are used to suppress the clutter returns. However, for the sake of completeness, basic non-parametric spectral estimation techniques are briefly covered.

Non-parametric spectral estimation methods, which are also known as classical spectrum estimation, are based on the Fourier transform of the data or its correlation function. It is named accordingly since the methods are applied directly to the observed data sequence and when the data sequence is long the spectral estimation performance of non-parametric methods are sufficient.

There are two non-parametric methods that are commonly used:

i. Periodogram,
ii. Correlogram.

During the development of spectral estimation techniques, these two methods are further developed to decrease the high variance at a cost of reduced

resolution of the estimates [14]. The most popular methods can be listed as follows;

i. Blackman-Tukey Method
ii. Bartlett Method
iii. Welch Method

In sub-sections of this section, basic information for these listed methods are given. Although all of the methods are very important and used widely in literature, more attention are given to periodogram and correlogram non-parametric spectral estimation methods.

3.2.1.1. Periodogram

The periodogram spectral estimation method relies on the second definition of PSD given in equation (3.4). In the formula, since finite amount of data is used, the expectation and limiting operations cannot be performed.

For finite amount of observations, $\{x(t)\}_{t=1}^{N}$, the periodogram method is used by the following formula;

$$\hat{\varphi}(\omega) = \frac{1}{N}\left|\sum_{t=1}^{N} x(t)e^{-j\omega t}\right|^2 . \tag{3.6}$$

The periodogram name comes from the fact that hidden periodicities are revealed [14]. In practical radar systems, the periodogram method is used for classical Doppler processing in the FFT blocks.

In the thesis, to compare the spectral estimation performance of parametric methods with the non-parametric ones, periodogram is used to estimate the spectral analysis of the signal.

3.2.1.2. Correlogram

The correlogram spectral estimation method is based on the first definition of PSD given in equation (3.2). However, since there exists finite amount of data and the covariance is unknown, the sum operation is taken within the finite set and estimation of covariance lag is used. The correlogram spectral estimator is shown in equation (3.7).

$$\hat{\varphi}(\omega) = \sum_{k=-(N-1)}^{N-1} \hat{r}(k) e^{-j\omega k} \ . \tag{3.7}$$

In (3.7), $\hat{r}(k)$ is found from the finite set of observations $\{x(t)\}_{t=1}^{N}$. There are two common ways to estimate the covariance of the signal which are standard unbiased ACS estimator or standard biased ACS estimator, and the expressions of these estimators are given in equation (3.8) and equation (3.9), respectively.

$$\hat{r}(k) = \frac{1}{N-k} \sum_{t=k+1}^{N} x(t) x^*(t-k) \qquad 0 \le k \le N-1. \tag{3.8}$$

$$\hat{r}(k) = \frac{1}{N} \sum_{t=k+1}^{N} x(t) x^*(t-k) \qquad 0 \le k \le N-1. \tag{3.9}$$

Since $\hat{r}(-k) = \hat{r}^*(k)$, the negative lags are easily obtained from equations (3.8) and (3.9). In order to guarantee the positive semi-definiteness of covariance matrix and to decrease the variance at the cost of increasing the bias of the estimation, standard biased ACS estimator is preferred among the two [14].

3.2.1.3. Blackman-Tukey Method

Blackman-Tukey spectral estimator merely corresponds to weighted average of the periodogram [14]. It is developed to reduce the statistical variability of periodogram method.

In (3.10), the formula for Blackman-Tukey method is shown;

$$\hat{\varphi}(\omega) = \sum_{k=-(M-1)}^{(M-1)} \omega(k)\hat{r}(k)e^{-j\omega k} \,. \tag{3.10}$$

Here, $w(k)$ is used to represent the windowing function which is even and zero outside the summation operation. Since $w(k)$ weights the lags of the sample covariance sequence, it is also called a lag window. One of the facts for Blackman-Tukey spectral estimation is that if the lag window is positive semi-definite, the estimated spectrum becomes positive for all frequencies [14].

Some of the common lag windows used for Blackman-Tukey spectral estimator method is shown in Table 3-1 [14].

Table 3-1: Common Windows used in Blackman-Tukey Method

Window Name	**Equation**	**Sidelobe Level (dB)**
Rectangular	$w(k) = 1$.	-13
Bartlett	$w(k) = (M-k)/M$.	-25
Hanning	$w(k) = 0.5 + 0.5\cos(\pi k/M)$.	-31

Table 3-2: continued

Hamming	$w(k) = 0.54 + 0.46\cos\left(\pi k / (M-1)\right)$.	-41
Blackman	$w(k) = 0.42 + 0.5\cos\left(\pi k / (M-1)\right) + 0.08\cos\left(2\pi k / (M-1)\right)$.	-57

Blackman-Tukey method smoothes the high variances in periodogram spectral estimation method but at the cost of reducing resolution.

3.2.1.4. Bartlett Method

Like Blackman-Tukey algorithm, the Bartlett method seeks to reduce the variance of periodogram estimator by splitting up the available sample of N observations into $L = N/M$ subsamples of M observations and average the individual periodograms. The sample splitting method is illustrated below.

$$\underbrace{x(1), x(2), \cdots, x(M)}_{\{x_1(n)\}}, \overbrace{x(M+1), \cdots x(K+M)}^{\{x_2(n)\}}, \cdots, x(N)$$

The mathematical representation of the Bartlett method is as follows;

$$x_j(t) = x((j-1)M + t) \qquad \begin{matrix} t = 1, \ldots, M \\ j = 1, \ldots, L \end{matrix}. \qquad (3.11)$$

denote the observation of j-th individual observation. Periodogram spectral estimation, which is shown in equation (3.12) is applied on this individual observation.

$$\hat{\phi}_j(w) = \frac{1}{M}\left|\sum_{t=1}^{M} x_j(t) e^{-jwt}\right|^2 . \tag{3.12}$$

The Bartlett spectral estimation is finally given by

$$\hat{\phi}(w) = \frac{1}{L}\sum_{j=1}^{L} \hat{\phi}_j(w). \tag{3.13}$$

Since the Bartlett method is applied on data segments of length $M = N/L$, the resolution that can be reached is reduced by a factor L; in other words, the resolution afforded should be on the order of $1/M$. In return, the Bartlett method has a reduced variance than the periodogram method.

3.2.1.5. Welch Method

Like Blackman-Tukey and Bartlett methods, the Welch method is used to reduce the variance in periodogram spectral estimation method at the cost of reducing resolution. For this purpose, in Welch method, first the observation data segments which are allowed to overlap are generated like Bartlett method. Then, each data segment is windowed prior to computing the periodogram. For these reasons, the Welch method can be considered as a refined form of Bartlett method. The overlapping windows for Welch method is shown below.

$$\begin{aligned}
&x(1), x(2), \cdots, x(K), x(K+1), \cdots, x(M), x(M+1), \cdots, x(K+M), \cdots, x(N) \\
&\{x_1(n)\} = x(1), \cdots, x(M) \\
&\{x_2(n)\} = x(K), \cdots, x(K+M) \\
&\vdots
\end{aligned}$$

The Welch method can be described by the following mathematical equations;

$$x_j(t) = x((j-1)K + t) \qquad \begin{matrix} t = 1,\ldots,M \\ j = 1,\ldots,S \end{matrix} . \tag{3.14}$$

where j denotes the j[th] data segment. If $K = M$, the sequences do not overlap and the sample splitting of Bartlett method is obtained. If $K = M/2$, 50 % overlapping (or 75 % overlapping) which is commonly preferred [14] is obtained.

The windowed periodogram corresponding to $x_j(t)$ is expressed in equation (3.15).

$$\hat{\varphi}_j(\omega) = \frac{1}{PM}\left|\sum_{t=1}^{M} v(t)x_j(t)e^{-j\omega t}\right|^2 . \tag{3.15}$$

Here, P which is required for the periodogram estimate to become asymptotically unbiased, denotes the power of temporal windows, $\{v(t)\}$ and is obtained as follows;

$$P = \frac{1}{M}\sum_{t=1}^{L}|v(t)|^2 . \tag{3.16}$$

Finally, the Welch spectral estimate is found by averaging individual periodograms of sample segments.

$$\hat{\varphi}(\omega) = \frac{1}{S}\sum_{j=1}^{S}\hat{\varphi}_j(\omega). \tag{3.17}$$

The modifications in Bartlett method to obtain the Welch method are apparent. By allowing the overlap between the data segments more periodograms are determined; hence, the variance of spectral estimation is reduced. Moreover, the window in the periodogram computation gives more control over the bias property of spectral estimation. Furthermore, by arranging the weights of the temporal window (i.e. giving less weights to ends of the sample sequence), less correlation among overlapped sequences are made and the variance in spectral estimation is reduced [14].

3.2.2. Parametric Spectral Estimation

In non-parametric spectral estimation methods covered previously, except stationarity of signals that are studied, no assumptions are made for its power spectral density. However, in parametric methods it is assumed that the power spectral density of the signal under study satisfies a certain functional form and the spectral estimation is carried out to determine parameters in the signal model. That is why parametric methods are also regarded as model-based methods.

The parametric methods which are covered in this section are;

- Autoregressive Moving Average (ARMA)
- Autoregressive (AR)
- Moving Average (MA)

spectral estimation methods. Among these parametric estimation methods, it is appropriate to model spectra with sharp peak as AR model (i.e. narrowband signal), spectra with deep valleys as MA model (i.e. wideband signal) and a spectra with deep valleys and sharp peaks with ARMA model [15].

Before giving basic information on these parametric spectral estimation methods, it is appropriate to define the rational transfer function of signals.

It is known that the PSD of many discrete-time random processes encountered in practice are well approximated by a rational transfer function model [15]. A rational PSD function of $e^{-j\omega}$ is given in equation (3.18).

$$\varphi(\omega)=\frac{\sum_{k=-m}^{m}\gamma_k e^{-j\omega k}}{\sum_{k=-n}^{n}\rho_k e^{-j\omega k}}. \tag{3.18}$$

where $\gamma_{-k}=\gamma_k^*$ and $\rho_{-k}=\rho_k^*$. It is assured in The Weierstrass Theorem from calculus that if m and n are chosen sufficiently large, any continuous PSD (and some discontinuous PSD) can be approximated by a rational PSD. That is, the rational PSDs form a dense set in the class of continuous spectra [14].

Since power spectral density is a positive function, $\phi(w)\geq 0$, the factorization of the PSD can be used.

$$\varphi(\omega)=\left|\frac{B(\omega)}{A(\omega)}\right|^2\sigma^2. \tag{3.19}$$

where σ^2 is a positive scalar, $A(w)$ and $B(w)$ are the polynomials;

$$\begin{aligned}A(\omega)&=1+a_1e^{-j\omega}+a_2e^{-j2\omega}+\ldots+a_ne^{-j\omega w}\\ B(\omega)&=1+b_1e^{-j\omega}+b_2e^{-j2\omega}+\ldots+b_me^{-j\omega w}\end{aligned}. \tag{3.20}$$

Hence, expressing equations in (3.19) and (3.20) in z-domain and using spectral factorization theorem (the fact that the poles and zeros are in symmetric pairs about the unit circle), it can be shown that any signal having a

rational PSD can be obtained by filtering white noise of power σ^2 through the rational transfer function $H(\omega)=B(\omega)/A(\omega)$.

$$e(t)\rightarrow \boxed{H(\omega)=\frac{B(\omega)}{A(\omega)}}\rightarrow y(t) \tag{3.21}$$

Or alternatively;

$$A(q)y(t)=B(q)e(t). \tag{3.22}$$

Here, $y(t)$ is the filter output, $e(t)$ is the white noise with variance σ^2 and q is the unit delay operator. With this PSD model, the spectral estimation is turned into a signal modeling problem. For different values of m and n given in (3.20), the name of the modeling changes. That is for $m=0$ the model is AR, for $n=0$ the model is MA and if m and n are both non-zero the signal model is called as ARMA.

Hence, the PSD in normalized frequency and corresponding difference equations for ARMA, AR and MA processes are given in equations below.

$$\begin{aligned}
&\phi_{ARMA}(f)=\sigma^2\left|\frac{B(f)}{A(f)}\right|^2 \Rightarrow A(q)y(t)=B(q)e(t)\\
&\phi_{AR}(f)=\sigma^2\left|\frac{1}{A(f)}\right|^2 \Rightarrow A(q)y(t)=e(t) \qquad -1/2\le f\le 1/2.\\
&\phi_{MA}(f)=\sigma^2|B(f)|^2 \Rightarrow y(t)=B(q)e(t)
\end{aligned} \tag{3.23}$$

Here, $A(f)$ denotes $A(e^{j2\pi f})$ and $B(f)$ denotes $B(e^{j2\pi f})$.

In the next subsections, the basic characteristics and of the ARMA signals, AR signals and MA signals are covered.

3.2.2.1. Autoregressive Moving Average Signals

The ARMA process is generated by filtering white noise with a filter which has m zeros and n poles discussed in previous section. Since in the PSD of ARMA process the zeros and poles appear in symmetric pairs, there exists $2m$ zeros and $2n$ poles. The ARMA filter shown in equation (3.21) can be expressed in z-domain as follows;

$$H(z)=\frac{B(z)}{A(z)}=\frac{\sum_{k=0}^{m} b_k z^{-k}}{1+\sum_{k=1}^{n} a_k z^{-k}}. \tag{3.24}$$

where $a_0 = 1$. The power spectrum density of $\phi(z)$ in z-domain can be written by assuming the power spectrum of white noise is σ^2.

$$\phi(z)=|H(z)|^2\sigma^2=\frac{B(z)B^*(1/z)}{A(z)A^*(1/z)}\sigma^2. \tag{3.25}$$

Equation (3.25) can be expressed as follows;

$$\phi(z)A(z)=\frac{B^*(1/z)}{A^*(1/z)}B(z)\sigma^2. \tag{3.26}$$

$$\phi(z)A(z)=H^*(1/z)B(z)\sigma^2. \tag{3.27}$$

By taking the inverse z-transform of both sides, the following relations are obtained.

$$F^{-1}\{\phi(z)A(z)\} = F^{-1}\{H^*(1/z)B(z)\sigma^2\}. \tag{3.28}$$

$$\sum_{l=0}^{n} a_l r(k-l) = \sigma^2 \sum_{l=0}^{m} b_l h^*(l-k). \tag{3.29}$$

It is already known that the filter $H(z)$ is causal and stable, which means $h(k)=0$ for $k<0$. Hence, the result of ARMA process becomes as follows;

$$r(k) = \begin{cases} -\sum_{l=1}^{n} a_l r(k-l) + \overbrace{\sigma^2 \sum_{l=0}^{m-k} b_{l+k} h^*(l)}^{non-linearity} & k = 0,1,\ldots,m \\ -\sum_{l=1}^{n} a_l r(k-l) & k > m \end{cases}. \tag{3.30}$$

which in matrix form becomes as follows;

$$\begin{bmatrix} r(0) & r(-1) & \cdots & r(-n) \\ r(1) & r(0) & \cdots & r(-n+1) \\ \vdots & \vdots & \vdots & \vdots \\ r(m) & r(m-1) & \cdots & r(m-n) \\ r(m+1) & r(m) & \cdots & r(m-n+1) \\ \vdots & \vdots & \vdots & \vdots \\ r(m+n) & r(m+n-1) & \cdots & r(m) \end{bmatrix} \begin{bmatrix} 1 \\ a_1 \\ a_2 \\ \vdots \\ a_n \end{bmatrix} = \sigma^2 \begin{bmatrix} \sum_{l=0}^{m} b_l h^*(l) \\ \sum_{l=1}^{m} b_l h^*(l-1) \\ \vdots \\ \sum_{l=n}^{m} b_l h^*(l-n) \\ 0 \\ \vdots \\ 0 \end{bmatrix}. \tag{3.31}$$

After finding the autoregressive parameters a_k from p linear equations in (3.31), the moving average parameters b_k can be determined from a_k values. Let c_k be the convolution between b_k and $h^*(-k)$.

$$c_k = b_k \otimes h^*(-k). \tag{3.32}$$

Since $c_k = 0$ for $k > m$, the sequence is known for all $k \geq 0$. The causal part of c_k may be written by $[C(z)]_+$,

$$[C(z)]_+ = \sum_{k=0}^{\infty} c_k z^{-k} . \tag{3.33}$$

Similarly, the anticausal part of c_k is $[C(z)]_-$,

$$[C(z)]_- = \sum_{k=-\infty}^{-1} c_k z^{-k} . \tag{3.34}$$

We know that c_k is the convolution of b_k and $h^*(-k)$. Thus,

$$C(z) = B(z)H^*(1/z) = B(z)\frac{B^*(1/z)}{A^*(1/z)}. \tag{3.35}$$

Multipliying $C(z)$ with $A^*(1/z)$, we obtain the power spectrum of MA process.

$$P(z) = C(z)A^*(1/z) = B(z)B^*(1/z). \tag{3.36}$$

Since a_k is zero for $k < 0$, $A^*(1/z)$ contains only positive powers of z. Therefore,

$$P(z) = C(z)A^*(1/z) = [C(z)]_+ A^*(1/z) + [C(z)]_- A^*(1/z). \tag{3.37}$$

Since both $[C(z)]_-$ and $A^*(1/z)$ are polynomials that contain only positive powers of z, the causal part of $P(z)$ is equal to;

$$[P(z)]_+ = [[C(z)]_+ A^*(1/z)]_+ \tag{3.38}$$

Hence, although c_k is unknown for $k < 0$, the causal part of $P(z)$ may be computed from the causal part of c_k and a_k. Finally, using conjugate symmetry of $P(z)$, we may determine $P(z)$, i.e. the spectrum of MA process, for all z.

3.2.2.2. Autoregressive Signals

Autoregressive process is a type of ARMA process when the filter $H(z)$ has n poles and no zeros. The estimation of parameters in AR signal can be found by solving a set of linear equations, which is called Yule-Walker equation set.

For AR signals, the filter response becomes as follows;

$$H(z) = \frac{B(z)}{A(z)} = \frac{b_0}{1 + \sum_{k=1}^{n} a_k z^{-k}}. \tag{3.39}$$

The output AR signal has the power spectrum as follows;

$$\phi(z) = |H(z)|^2 \sigma^2 = \frac{|b_0|^2}{A(z)A^*(1/z)} \sigma^2. \tag{3.40}$$

The linear Yule-Walker equation set is obtained by solving equation (3.30) for $m = 0$.

$$r(k)=\begin{cases}-\sum_{l=1}^{n}a_l r(k-l)+\sigma^2|b_0|^2 & k=0,\\ -\sum_{l=1}^{n}a_l r(k-l) & k>0\end{cases}. \tag{3.41}$$

In matrix form, the Yule-Walker linear equation set can be written in augmented form as follows;

$$\begin{bmatrix} r(0) & r(-1) & \cdots & r(-n) \\ r(1) & r(0) & \cdots & r(-n+1) \\ \vdots & \vdots & \vdots & \vdots \\ r(n) & r(n-1) & \cdots & r(0) \end{bmatrix}\begin{bmatrix} 1 \\ a_1 \\ \vdots \\ a_n \end{bmatrix}=\sigma^2|b_0|^2\begin{bmatrix} 1 \\ 0 \\ \vdots \\ 0 \end{bmatrix}. \tag{3.42}$$

As mentioned earlier, the AR estimation which is used extensively during parametric spectral estimation methods is conducted using a set of linear equations. The algorithm steps for determining the AR spectral estimation is as follows;

i. Using the signal data vector $x(t)$ and standard biased ACS estimator, the ACS $\hat{r}(k)$ is determined.

$$r(k)=\frac{1}{N}\sum_{t=k+1}^{N}x(t)x^*(t-k). \tag{3.43}$$

ii. The AR filter coefficients $\theta=[a_1 \quad a_2 \quad \cdots \quad a_n]$ are estimated from the set of equations $r_n+R_n\theta=0$, which is written in matrix form as follows;

$$\underbrace{\begin{bmatrix} r(1) \\ \vdots \\ r(n) \end{bmatrix}}_{r_n} + \underbrace{\begin{bmatrix} r(0) & \cdots & r(-n+1) \\ \vdots & \ddots & \vdots \\ r(n-1) & \cdots & r(0) \end{bmatrix}}_{R_n} \underbrace{\begin{bmatrix} a_1 \\ \vdots \\ a_n \end{bmatrix}}_{\theta} = \begin{bmatrix} 0 \\ \vdots \\ 0 \end{bmatrix}. \tag{3.44}$$

iii. Estimate the noise variance σ^2 from the estimated ACS and AR filter parameters.

$$r(0) + \sum_{k=1}^{n} a_k r(-k) = \sigma^2 \ . \tag{3.45}$$

3.2.2.3. Moving Average Signals

Moving Average process is a type of ARMA process when the filter $H(z)$ has m zeros and no poles. Like AR signals, MA signals are obtained by filtering white noise with FIR filter, shown in equation (3.46).

$$H(z) = B(z) = \sum_{k=0}^{m} b_k z^{-k} \ . \tag{3.46}$$

Thus, the power spectrum of MA signals become as follows;

$$\phi(z) = |H(z)|^2 \sigma^2 = \sigma^2 B(z) B^*(1/z). \tag{3.47}$$

Here, σ^2 is the input noise variance. Although unlike the AR parameter estimation, MA parameter estimation is a non-linear one, the Yule-Walker equations can be written by writing $a_k = 0$ and $h(k) = b_k$ for any k into equation (3.31).

$$r(k) = \sigma^2 \sum_{l=1}^{m-|k|} b_{l+|k|} b_l^* \ . \tag{3.48}$$

where ACS $r(k)$ can be determined from standard biased ACS estimator given in equation (3.9).

3.2.3. Model Order Selection Criteria

The model order selection is one of the most important aspects of using parametric spectral estimation methods. As a general rule, if the order of the parametric method is too low, a highly smoothed spectrum having low resolution is obtained. On the other hand, if the order is too high, the estimation performance would degrade due to spurious low-level peaks in the spectrum and cause general statistical instability [16].

The performance of parametric spectral estimators can be determined by mean square error (MSE) of the residual error. The residual errors can vary with the order selection is done by minimizing the AIC (with respect to p,q, or both) given in equations (3.43), (3.44), and (3.45) for AR, MA and ARMA models, respectively. Accordingly, by investigating the residual errors for different orders, the model order can be selected. However, this approach may be imprecise and ill defined [16]. Hence, for AR, MA and ARMA spectral estimators, different methods are investigated in literature.

For selecting model order criterion, two well known approaches have been proposed Akaike (1969, 1974). These approaches are: *Final Prediction Error (FPE) Criterion* and *Akaike Information Criterion (AIC)*.

These two approaches are originally developed for AR spectral estimator but *AIC* can be developed for MA and ARMA spectral estimators.

For an *AR(p)* spectral estimator where *p* is the model order, in *FPE* the order is selected to minimize the performance index given as [16]:

$$FPE(p) = \sigma_{wp}^2 \left(\frac{N + p + 1}{N - p - 1} \right). \tag{3.49}$$

where N is the input signal length, and σ_{wp}^2 is the estimated variance of the linear prediction error. The basic idea in performance index is to minimize the mean square error (MSE) for a one step predictor [16].

In *AIC*, for *AR(p)*, *MA(q)* and *ARMA(p,q)* parametric spectral estimators, the minimization for selected order is based on the following relation for AR*(p)*, *MA(q)* and *ARMA(p,q)* estimators given in equations (3.50), (3.51) and (3.52) respectively:

$$AIC(p) = \ln \sigma_{wp}^2 + \frac{2p}{N}. \tag{3.50}$$

$$AIC(q) = \ln \sigma_{wp}^2 + \frac{2q}{N}. \tag{3.51}$$

$$AIC(p,q) = \ln \sigma_{wp}^2 + \frac{2(p+q)}{N}. \tag{3.52}$$

In all criteria, it can easily be seen that the term σ_{wp}^2 decreases, as the model orders increases. However, as the model order increases beyond a certain value, the 2nd terms in the equations become dominant and AIC increases. Hence, the optimum model order for a spectral estimator is obtained by searching for minimum *AIC* values.

Finally, for AR spectral estimator, two more criteria for choosing model order can be found in literature: the *minimization of description length* (MDL) and the *criterion autoregressive transfer* (CAT) [16]. However, since these methods are not commonly used, they are not covered in this report.

CHAPTER 4

SIMULATION RESULTS

4.1. Simulation Assumptions

In this chapter, the modeling performance of ARMA spectral estimator for different clutter parameters and ARMA model orders are investigated. In the simulations, the clutter parameters and ARMA model orders are varied to better examine the performances. In this section, the assumptions taken are given briefly.

First of all, the simulations are presented in three sub-sections for different clutter covariance matrix types. These are exponential covariance matrix, Gaussian covariance matrix, and Gaussian covariance matrix tapered with internal clutter motion (hence the resulting covariance matrix is neither exponential nor Gaussian).

An exponential ACF arises from internal clutter motion, [12], and the corresponding covariance matrix is defined by the single parameter, ρ_E, which is called the correlation coefficient for exponential clutter. Since the internal clutter motion depends mainly on the environmental and radar parameters (carrier frequency, wind velocity, etc), ρ_E is varied between 0.9 and 0.99 in the simulations whenever internal clutter motion is dominant. For a radar

operating with 10GHz carrier frequency, the correlation coefficient 0.9 and 0.99 corresponds to wind velocities of 10.3 miles per hour (mph) and 9.65 mph, respectively [11].

A Gaussian ACF arises from the antenna scanning modulation, as mentioned in previous chapters. To generate Gaussian covariance matrix, the radar parameters are set as follows: 30 rpm antenna angular rotation speed, 5 kHz pulse repetition frequency (PRF) and a 3-dB antenna beam-width of 2°. The covariance matrix resulting from these radar parameters are determined using equations given in Chapter 2. The correlation coefficient resulting from these radar parameters equals to 0.99.

The K-distributed clutter shape parameter is also varied in the simulations. That is, the shape parameter is varied between 0.1, corresponding to a spiky clutter and 10 corresponding to a non-spiky clutter.

Finally, the CNR and number of processed pulses are varied to see its effect on the performance. The values of CNR and number of processed pulses used in the simulations are 20 dB and 64, respectively. Moreover, the pole and zero orders of the ARMA model are taken as the same.

4.2. Simulations for ARMA Model Order Selection

As given in Chapter 2, clutter contains a lot of parameters that affect the estimation performance. For this purpose, we investigate the ARMA spectral estimation performance in modeling K-distributed clutter in the presence of thermal noise.

To evaluate the performance of ARMA estimators with different orders, the root mean squared (RMS) error in estimations is determined. The RMS error is defined as:

$$E_{rms} = \sqrt{\frac{1}{N}\sum_{f=-0.5}^{0.5}\left(\Phi_{ARMA}(f) - \Phi_{CLUT}(f)\right)^2}\ . \tag{4.1}$$

where E_{rms} is the RMS error over Monte Carlo runs, Φ_{ARMA} is the estimated PSD with ARMA method, Φ_{CLUT} is the original clutter PSD, N is the number of Monte Carlo runs and f is the normalized frequency point with respect to the PRF which can be written as $f = f_d / PRF$ where f_d is the Doppler frequency in Hz and PRF is the radar pulse repetition frequency in Hz.

In the next sub-section, we investigate the performance of spectral estimators for clutter with exponential covariance matrix.

- **Clutter Signal Having Exponential ACS**

The exponential covariance matrix resulting from the internal clutter motion (ICM) has the structure given in equation (2.32). However, the correlation coefficient depends mainly on environmental conditions with stationary radar antenna assumption.

Before conducting the simulations, the PSD of an exponential signal is investigated. Let $x(t)$ be an exponential autocorrelation function (ACF) which can be written as follows:

$$x(t) = e^{-\alpha|t|}, \quad -\infty < t < \infty\ ,\ \alpha > 0 \tag{4.2}$$

It is well known that the Fourier Transform of this signal gives the power spectral density (PSD) of an exponential ACF.

$$X(\omega) = \int_{-\infty}^{\infty} e^{-\alpha|t|} e^{-j\omega t}\, dt\ . \tag{4.3}$$

$$X(\omega) = \int_{-\infty}^{0} e^{\alpha t} e^{-j\omega t} dt + \int_{0}^{\infty} e^{-\alpha t} e^{-jwt} dt \,. \tag{4.4}$$

By taking the above integral, the following relation for Fourier Transform of exponential signal is obtained.

$$X(\omega) = \frac{1}{\alpha - j\omega} + \frac{1}{\alpha + j\omega} = \frac{2\alpha}{\alpha^2 + \omega^2} \,. \tag{4.5}$$

From equation (4.5), it is observed that exponential signals can be modeled well by an AR(1) process.

In order to see the modeling performance of signal with exponential ACS with AR(1) process, the PSD of a signal with exponential ACF is obtained with a correlation coefficient equal to 0.99. As given previously, for a radar operating at 10 GHz carrier frequency, this correlation coefficient corresponds to a wind velocity of 9.65 mph. The PSD is obtained by taking the forward FFT of the first row of the covariance matrix and is shown in Figure 4-1 for FFT length of 1024 points and 64 coherent radar pulses.

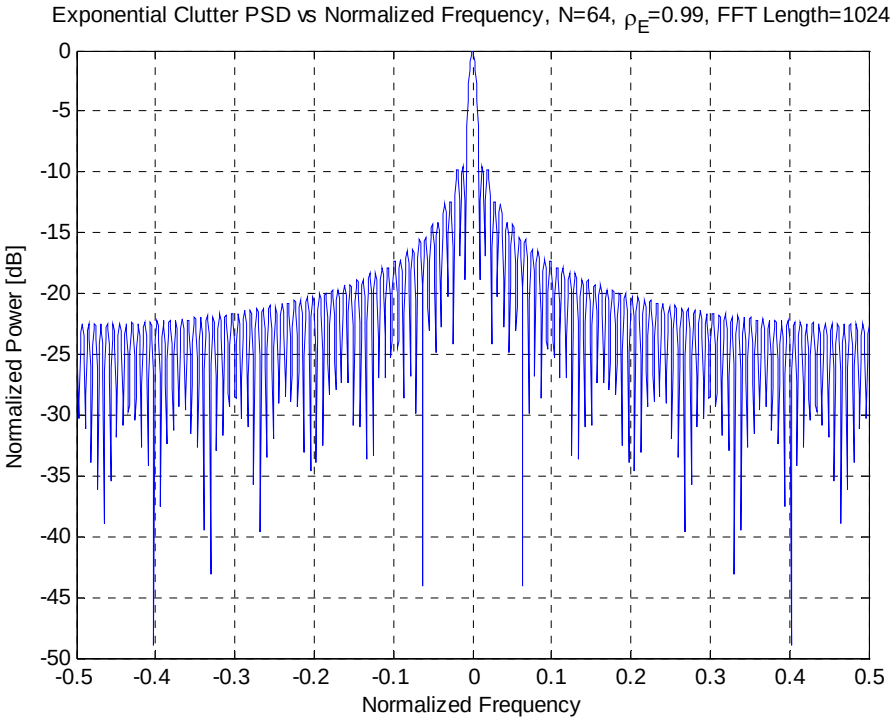

Figure 4-1: Clutter PSD for Signal with Exponential ACS

In order to see the PSD of a signal with exponentially decaying ACS, the figure is zoomed in Figure 4-2 around DC frequencies where most of the power is confined.

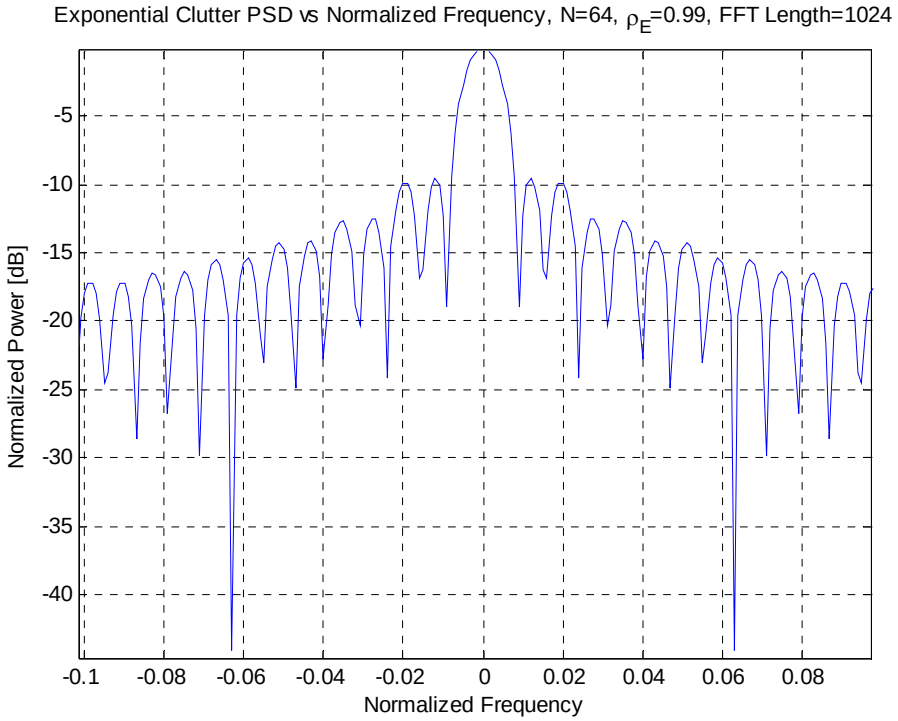

Figure 4-2: Clutter PSD for Signal with Exponential ACS, Zoomed Version

In (4.7), we see that AR(1) process can be model the signal with an exponential decaying ACS. In Figure 4-3, the PSD obtained by AR(1) process and PSD of a signal having exponential ACS are plotted together. In this figure, the ripples observed in the PSD of the signal having exponential ACS is the results of the finite number of pulses, which is 64 in our case, used in the simulation. However, we observe that AR(1) process well models the signals with exponentially decaying ACS.

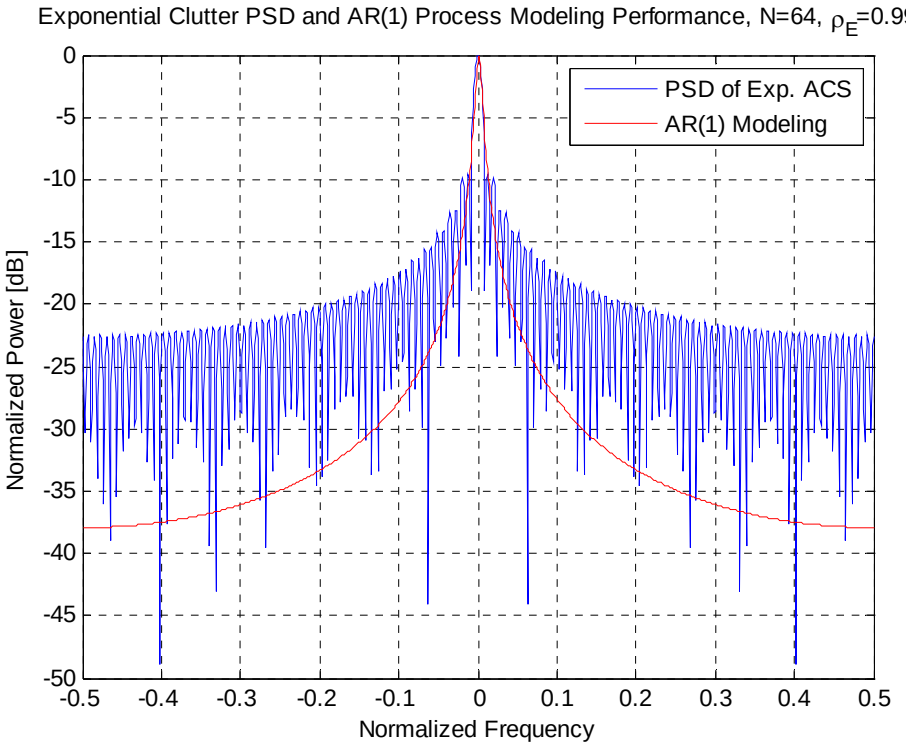

Figure 4-3: Clutter PSD for Signal with Exponential ACS and AR(1) Process Modeling

After the analytical investigation of a signal with exponential ACF, simulations are performed to see the ARMA modeling performance on signals having exponential ACF. Firstly, by making the number of processed pulses and the CNR values constant, we investigate the performance of the ARMA spectral estimator by varying the shape parameter from 0.1 to 10 for the K-distributed clutter. In the analysis, the CNR value is taken as 20dB, the number of processed pulses is 64, and the number of Monte Carlo runs is 1000. Moreover, the correlation coefficient for exponential clutter covariance matrix is taken as 0.95, which corresponds to a wind velocity of 9.9 mph for a radar with 10 GHz carrier frequency.

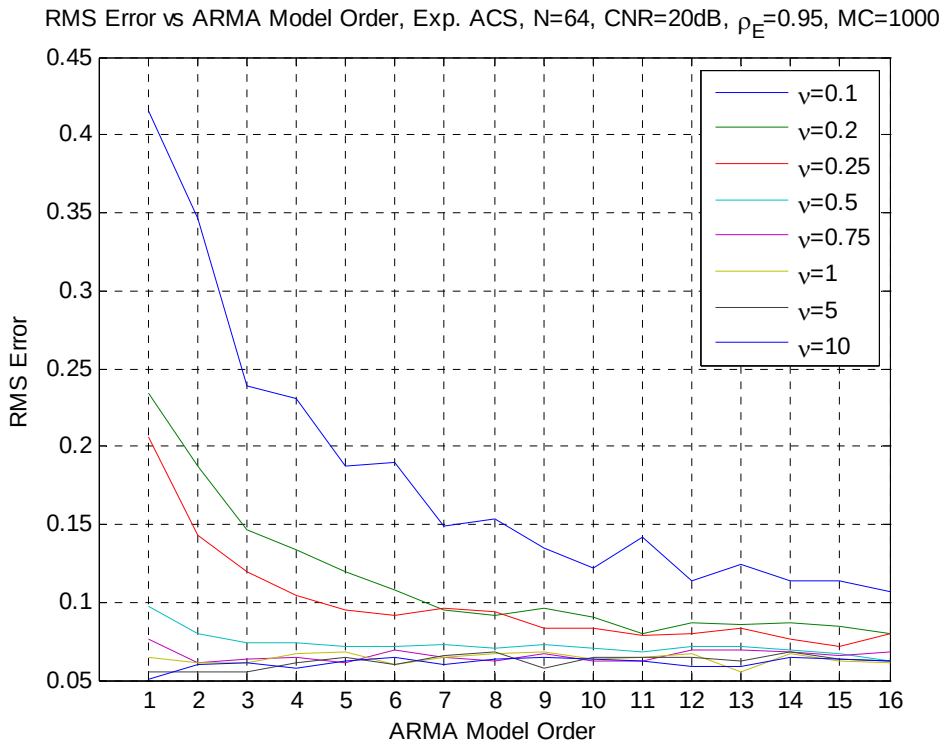

Figure 4-4: ARMA Spectral Estimator Performance for Different Values of the Shape Parameters (ν)

As seen from Figure 4-4, the RMS errors in modeling the spectrum of K-distributed clutter changes for different clutter shape parameters. We can make two observations from Figure 4-4. Firstly, we see that the RMS error decreases with increasing clutter shape parameter. From [2], we know that when the shape parameter is small, the clutter signal is spiky and is not characterized by Gaussian distribution but with K-distribution. As the shape parameter increases, the clutter signal can be characterized by Gaussian distribution. Although ARMA model does not depend on the input signal distribution, we see that the ARMA spectral estimator performs better for Gaussian distributed signals. This is because the standard biased ACS equation given in (3.8) is optimum for signals having Gaussian distribution. This result is also related to the problem of having finite amount of data. Therefore, we can conclude that

although the ARMA spectral estimator is independent from the distribution of an input signal, due to the ACS estimation conducted by equation (3.8), ARMA spectral estimator performs better for Gaussian distributed signals.

The second observation from Figure 4-4 is that as the ARMA model order increases, the RMS errors increase with ARMA model order for large shape parameters, whereas decrease for small shape parameters. We observe that the increase in the order of ARMA estimator performs differently for different shape parameters of signals having exponential ACS. When the shape parameter is small; i.e. when the signal is spiky and is not characterized by Gaussian distribution but with K-distribution, as the order of ARMA increases, the RMS error in the estimation decreases. This result can be interpreted as follows: since the standard ACS estimator is optimum for Gaussian distributed signals; the performance of the estimator is improved with increasing model order, due to the more accurate spectral estimation. However, when the shape parameter is large; i.e. the signal is Gaussian distributed, the RMS error increases with increasing ARMA model orders. This is due to the computational errors done in estimation with large ARMA model orders.

After observing the ARMA spectral estimator performance on signal having exponential ACS with different shape parameters, the ARMA spectral estimator performance is investigated for changing environmental conditions. Therefore, for spiky clutter signal having shape parameter 0.1 and Gaussian distributed clutter having shape parameter 10, the correlation coefficient of exponential ACS is varied. That is, the correlation coefficient is taken as 0.9, 0.95 and 0.99 corresponding to wind velocities of 10.3 mph, 9.9 mph and 9.65 mph for a radar with 10 GHz carrier frequency. In Figure 4-5, the RMS errors for different orders of ARMA obtained at two different K-distributed clutter shape parameters for several correlation coefficients are illustrated. In the simulation, the number of processed pulses is 64 and number of Monte Carlo runs is 1000.

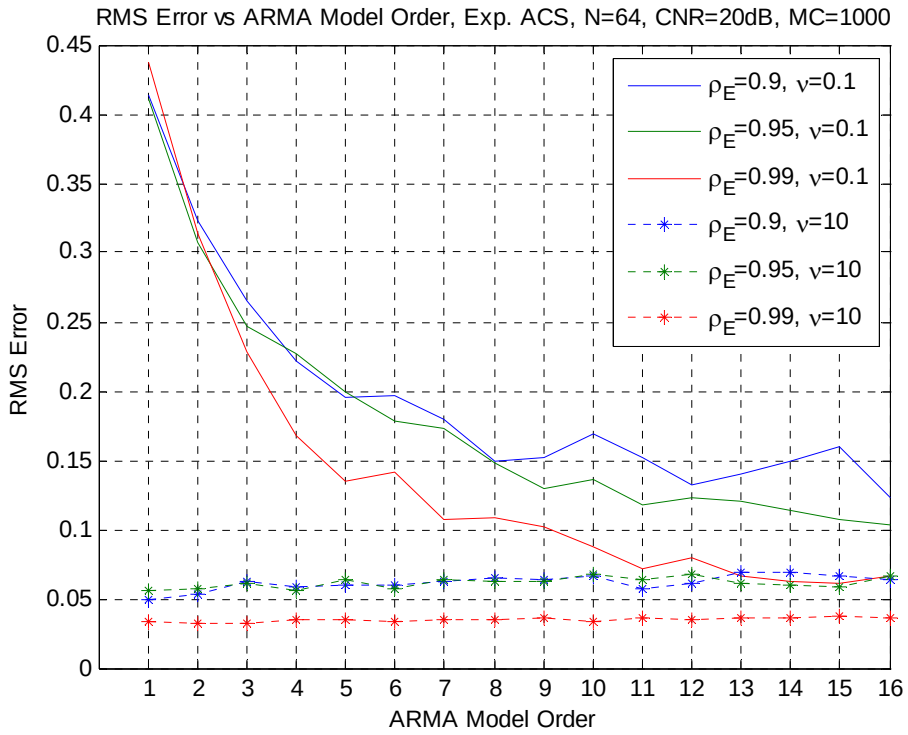

Figure 4-5: ARMA Spectral Estimator Performance for Different Correlation Coefficients at Clutter Shape Parameters (ν) 0.1 and 10

The results in Figure 4-5 show that, as the correlation coefficient increases, the ARMA performance increases independently from the distribution of the signal. This is due to the fact that the estimation performance increases as the correlation among signal samples increases since the estimation of ACS from correlated data becomes better.

In the next sub-section, we examine the performance of the ARMA estimator in the presence of clutter with a Gaussian ACS.

- **Clutter Signal Having Gaussian ACS**

The covariance matrix caused by Gaussian ACS results from the rotation of radar antenna and has the structure given in equation (2.27). It is well known that the power spectral density (PSD) of the clutter return within one range cell is determined by the corresponding covariance matrix. The original clutter PSD can be obtained by taking the inverse FFT of the first row of the covariance matrix. The original clutter PSD (normalized) is illustrated for 64 pulses and FFT length of 1024 in Figure 4-6. Moreover, the correlation coefficient of ACS is obtained from the radar parameters mentioned previously. The corresponding correlation coefficient equals to 0.99.

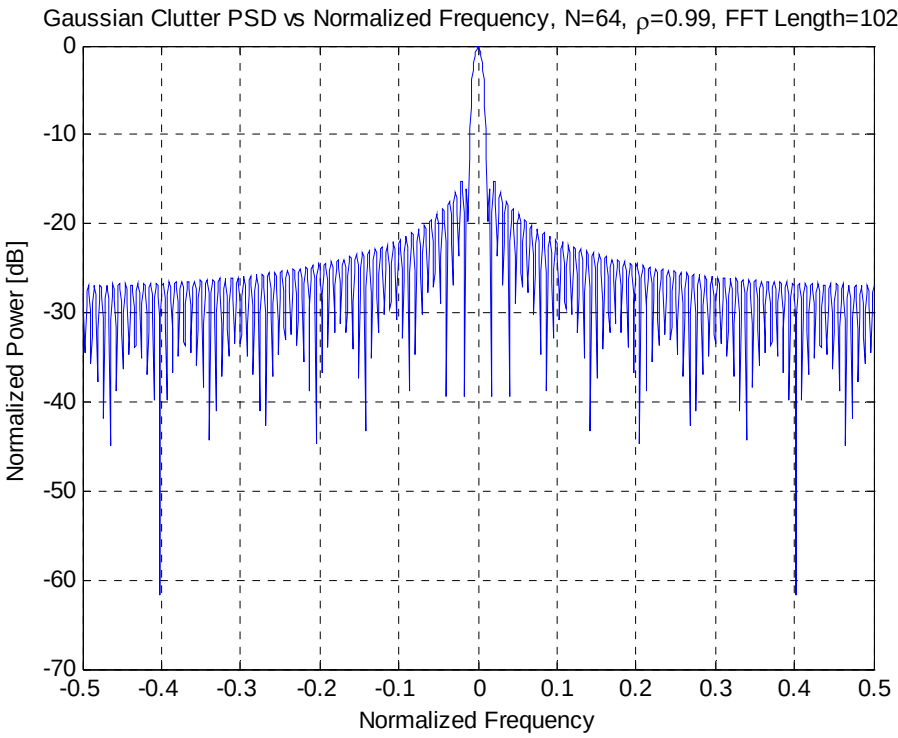

Figure 4-6: Clutter PSD for Signal with Gaussian ACS

In order to see PSD resulted from a Gaussian sequence, the figure is zoomed in Figure 4-7 around zero frequency (DC frequencies) where most of the power is confined.

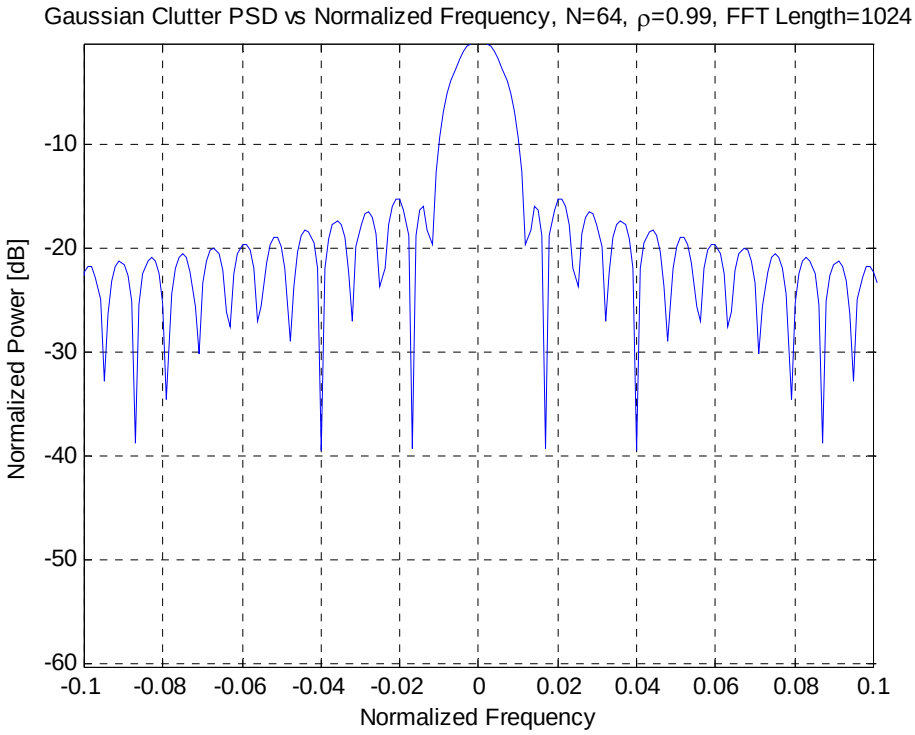

Figure 4-7: Clutter PSD for Signal with Gaussian ACS, Zoomed Version

Before going into the simulations, the analytical examination of a clutter signal having Gaussian ACS should be made. Let $x(t)$ be an Gaussian or bell-shaped autocorrelation function (ACF) which can be written as follows:

$$x(t) = e^{-\pi t^2}, \quad -\infty < t < \infty . \tag{4.6}$$

The Fourier Transform of this signal gives the power spectral density (PSD) of an Gaussian ACF.

$$X(\omega) = \int_{-\infty}^{\infty} e^{-\pi t^2} e^{-j\omega t} dt \,. \tag{4.7}$$

$$X(f) = \int_{-\infty}^{\infty} e^{-\pi\left(t^2 + j2ft\right)} dt = e^{\pi(jf)^2} \int_{-\infty}^{\infty} e^{-\pi\left[t^2 + j2ft + (jf)^2\right]} dt \,. \tag{4.8}$$

By taking the above integral, the following relation for Fourier Transform of exponential signal is obtained.

$$X(f) = e^{-\pi f^2} \int_{-\infty}^{\infty} e^{-\pi(t+jf)^2} d(t + jf) = e^{-\pi f^2} \,. \tag{4.9}$$

From equation (4.9), we observe that the PSD of a signal with Gaussian ACS is also Gaussian and does not have any poles or zeros. Therefore, unlike the signals with exponential ACS, an exact representation of Gaussian signal PSD with an ARMA model cannot be made. However, using Pade approximation, which is the best approximation of a function by a rational function, the PSD of a signal with Gaussian ACS can be modeled. In fact, ARMA(∞, ∞) can model the PSD of a signal with Gaussian ACS.

After mentioning the analytical behavior of a signal with Gaussian ACS, firstly, by making the number of processed pulses and CNR values constant, we examined the ARMA spectral estimator with different orders for different K-distributed clutter shape parameters. In the analysis, the CNR value is 20dB, the number of processed pulses is 64, and the number of Monte Carlo runs is 1000.

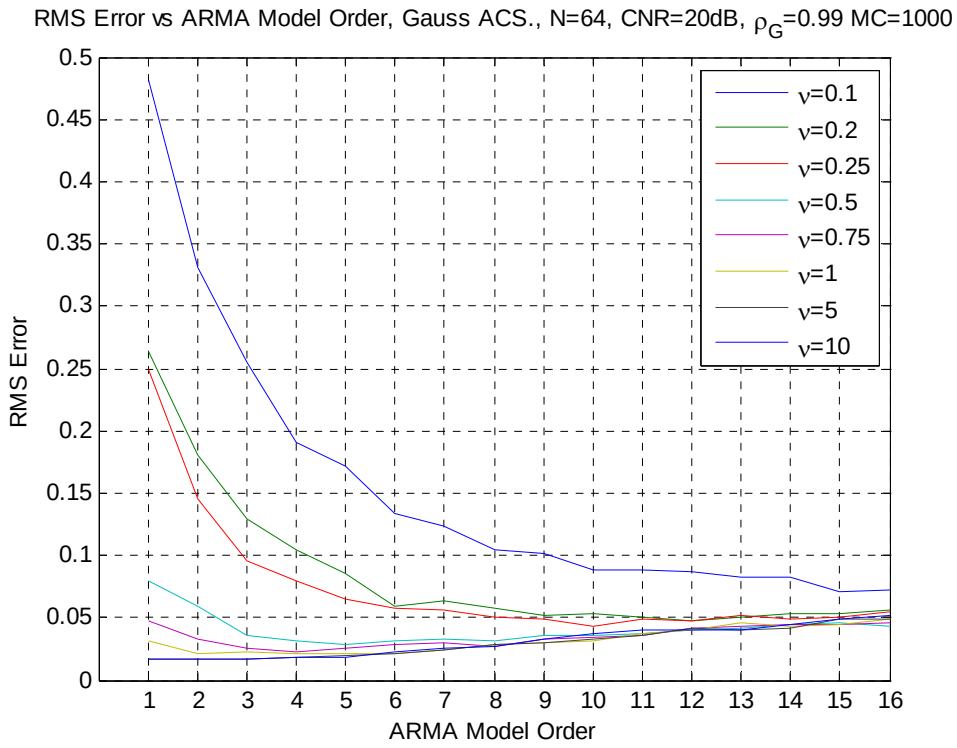

Figure 4-8: ARMA Spectral Estimator Performance for Different Values of the Shape Parameters (ν)

The results observed in Figure 4-8 is consistent with results obtained in exponential ACS. The RMS error in modeling the spectrum of K-distributed clutter changes for different clutter shape parameters. There are basically two observations from these results. Firstly, it is seen that RMS error decreases with increasing clutter shape parameter. Although no distribution information is required in ARMA spectral estimation, the ARMA spectral estimator performs better with Gaussian distributed clutter signals. This is due to the fact that the correlation sequence is estimated according to equation (3.8), which is the standard biased ACS estimator. This estimator is optimum for Gaussian signals; hence, the estimator performs better with input signals with Gaussian distribution. This is also related to the problem of having finite amount of data. Thus, we can conclude that although the ARMA spectral estimator is

independent from the distribution of an input signal, due to the ACS estimation conducted by equation (3.8), ARMA spectral estimator performs better for clutter signals having Gaussian ACS.

The other observation that we can make from Figure 4-8 is that as the ARMA model order increases, the RMS errors increase with ARMA model order for large shape parameters, whereas decrease for small shape parameters. The reason for this phenomenon is the same as discussed for clutter signals having exponential ACS. As the order of ARMA increases, the RMS error in the estimation decreases, when the shape parameter is small. This is because standard ACS estimator is optimum for Gaussian signals; as the order increases, the performance of the estimator is improved due to the more accurate estimation of higher order terms caused by spiky clutter signal. However, when the shape parameter is large, the RMS error increases with increasing ARMA model orders due to computational errors dominate in estimation of large ARMA orders and the use of less data to estimate the ACS for higher orders.

The performance of ARMA spectral estimator is also investigated for different CNR values. For this purpose, two shape parameters that yield K- and Gaussian-distributed clutter are considered. In Figure 4-9, the RMS error for different ARMA model orders obtained at two different clutter shape parameters for several CNR values are illustrated. In the simulation, the number of processed pulses is 64 and number of Monte Carlo runs is 1000.

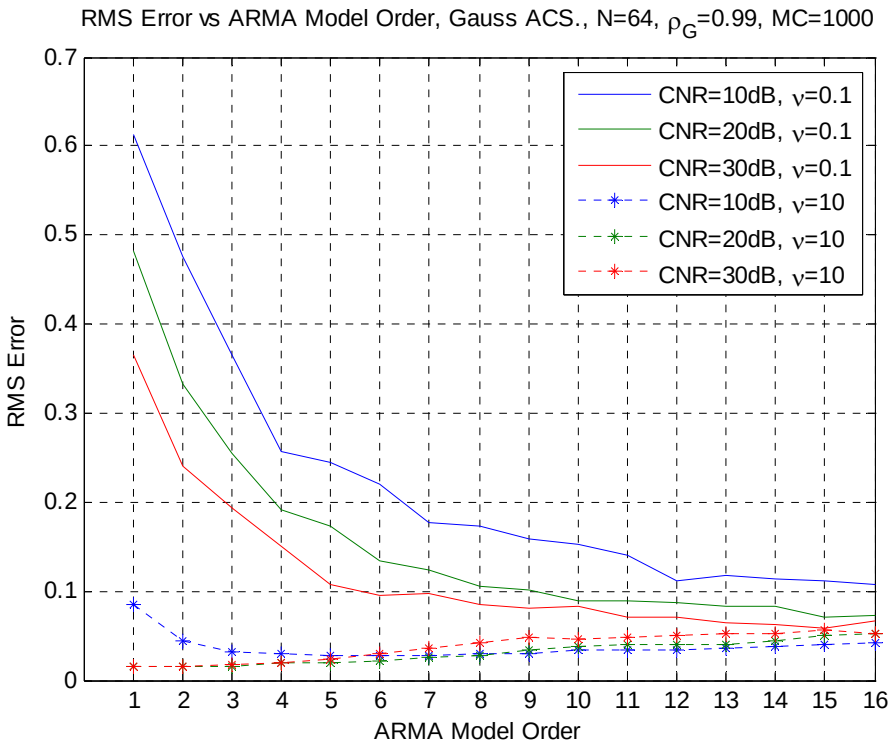

Figure 4-9: ARMA Spectral Estimator Performance for Different CNR Values at Clutter Shape Parameters (ν) 0.1 and 10

From above results, it is easily observed that for K-distributed clutter, as the clutter to noise ratio (CNR) increases, the effect of white Gaussian thermal noise decreases. As a result, the ARMA spectral estimation performance is improved with increasing CNR values. For spiky clutter signal, as the ARMA model order increases, the RMS error decreases since estimator is improved due to the more accurate estimation of higher order terms caused by spiky clutter signal. However, when the shape parameter is large; i.e. clutter signal is Gaussian distributed, as ARMA model order increases, the RMS error increases. The computational errors dominate in estimation of large ARMA orders and the use of less data to estimate the ACS for higher orders are the main reasons for this kind of behavior.

In the next sub-section, the ARMA estimator performance under clutter having Gaussian ACS tapered with internal clutter motion (ICM) is considered.

- **Clutter Signal Having Gaussian ACS tapered with ICM**

As mentioned previously, the signal having Gaussian ACS is resulted from antenna scanning modulation. In addition to this phenomenon, when the internal clutter motion affects the ACS, the resulting covariance matrix is tapered with ICM and is obtained by equation (2.34).

In the simulations, the radar parameters (3-dB beam-width, PRF, rpm) which are defined previously are kept fixed and the corresponding correlation coefficient is 0.99. However, the correlation coefficient resulted from ICM is varied in the simulations in order to observe different environmental conditions.

The original clutter PSD is obtained by taking the inverse FFT of the first row of covariance matrix, as done before. The original clutter PSD (normalized) is illustrated for 64 pulses and FFT length of 1024 in Figure 4-10. The correlation coefficient from ICM is taken as 0.99 and the correlation coefficient of Gaussian ACS equals to 0.99 in the simulation.

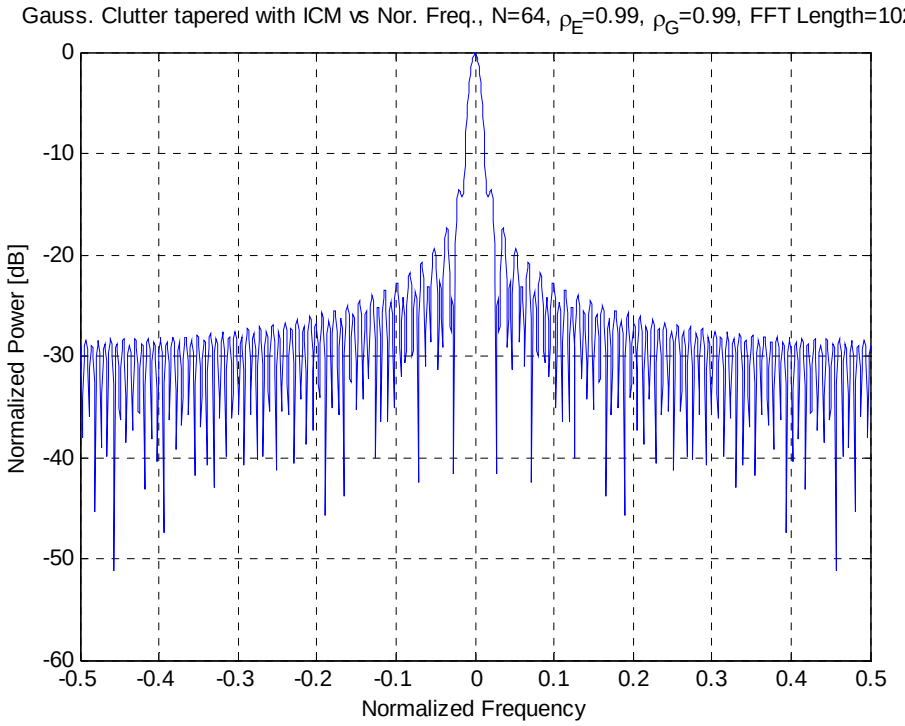

Figure 4-10: Clutter PSD for Gaussian Covariance Matrix tapered with ICM

In order to see the details of resulting PSD, the figure is zoomed in Figure 4-11 around zero frequency (DC frequencies) where most of the power is confined.

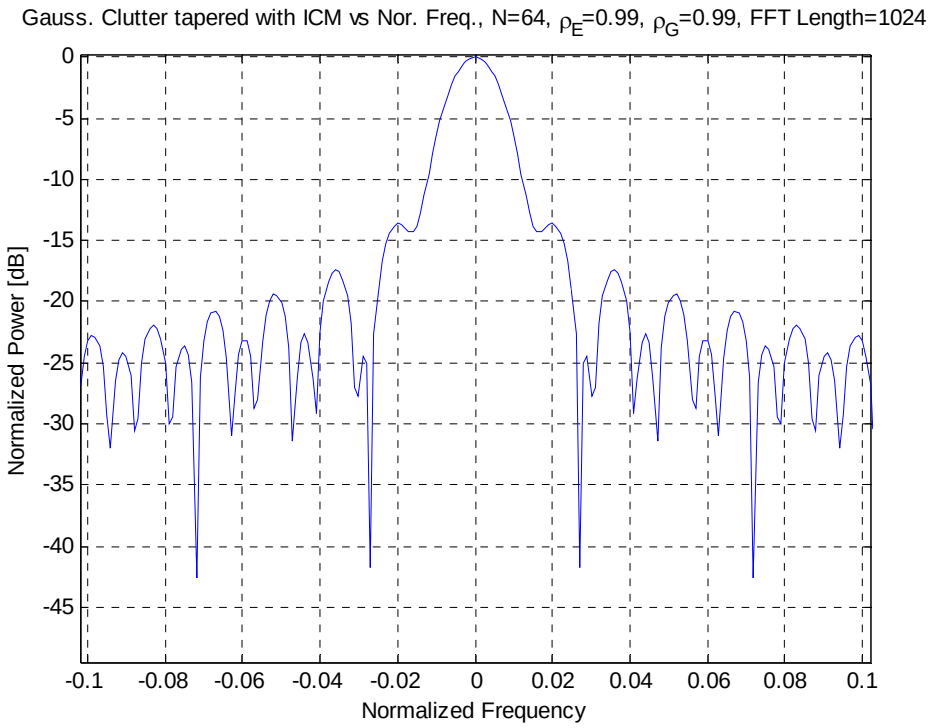

Figure 4-11: Clutter PSD for Gaussian Covariance Matrix tapered with ICM, Zoomed Version

Firstly, by making the number of processed pulses and CNR values constant, we investigate the ARMA spectral estimator of different orders for different K-distributed clutter shape parameter. In the analysis, the CNR value is taken as 20dB, the number of processed pulses is 64, and the number of Monte Carlo runs is 1000, and the correlation coefficient for exponential ACS due to ICM is taken as 0.95 corresponding to 9.9 mph wind velocity for a 10 GHz radar system.

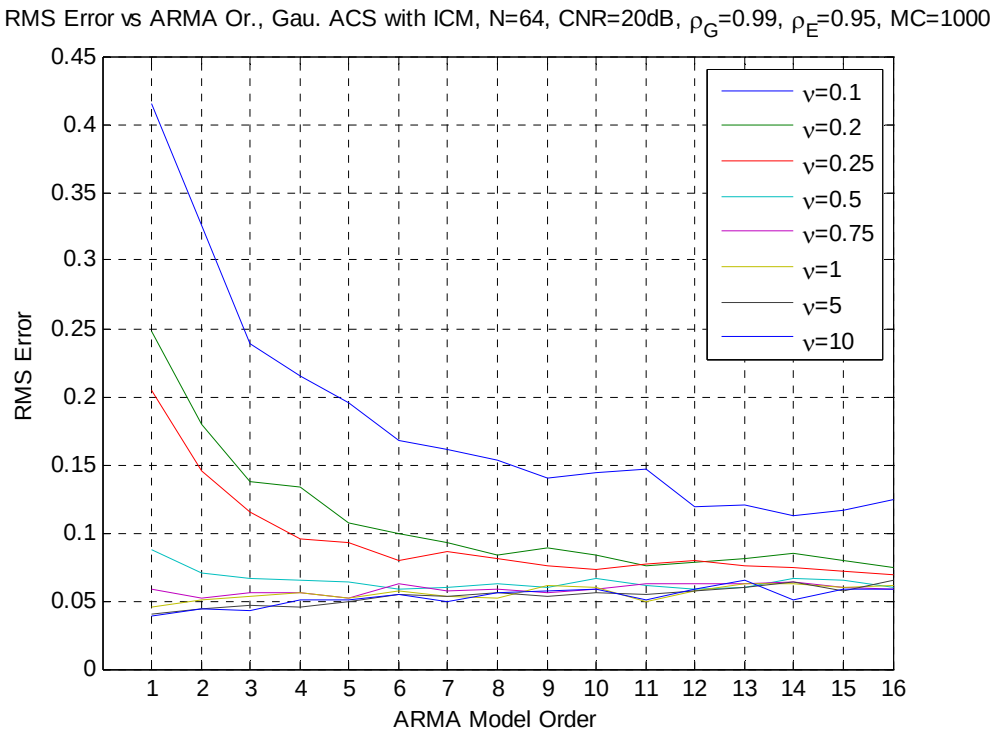

Figure 4-12: ARMA Spectral Estimator Performance for Different Values of the Shape Parameter (ν)

The results observed in Figure 4-12 is consistent with results obtained in previous simulations. There are again two observations that we can be derived from these results. First, we see that the RMS error decreases with increasing clutter shape parameter; that is, the ARMA spectral estimator performs better with Gaussian distributed clutter signals. From previous results, this observation is expected since the correlation sequence is estimated according to equation (3.8), which is the standard biased ACS estimator. It is obvious that estimator is optimum for Gaussian signals; thus, the estimator performs better with Gaussian distributed input signals. This result is also related to the problem of having finite amount of data. Therefore, it can be concluded that although the ARMA spectral estimator is independent from the distribution of an input signal, due to the ACS estimation conducted by equation (3.8),

ARMA spectral estimator performs better for clutter signals having Gaussian probability density function (PDF).

Secondly, from Figure 4-8, we see that as the ARMA model order increases, the RMS errors increase with ARMA model order for large shape parameters, whereas decrease for small shape parameters. As the order of ARMA increases, the RMS error in the estimation decreases when the shape parameter is small. The explanation is again the same at this point. The standard ACS estimator is optimum for Gaussian signals; as the order increases, the performance of the estimator is improved due to the more accurate estimation of higher order terms caused by spiky clutter signal. However, when the shape parameter is large, the RMS error increases with increasing ARMA model orders due to computational errors done in estimation of large ARMA orders and the use of less data to estimate the ACS for higher orders.

In addition to the previous simulation, the performance results for different correlation coefficient of ACS resulted from ICM is investigated for spiky and Gaussian clutter signals. That is, we investigate the ARMA spectral estimator performance for K- and Gaussian-distributed clutter returns; i.e. for shape parameters of 0.1 and 10, respectively, and we took the correlation coefficient as 0.9, 0.95 and 0.99. In Figure 4-13, the RMS error for different orders of ARMA obtained at two different clutter shape parameters for several correlation coefficients are illustrated. In the simulation, the number of processed pulses is 64 and number of Monte Carlo runs are 1000.

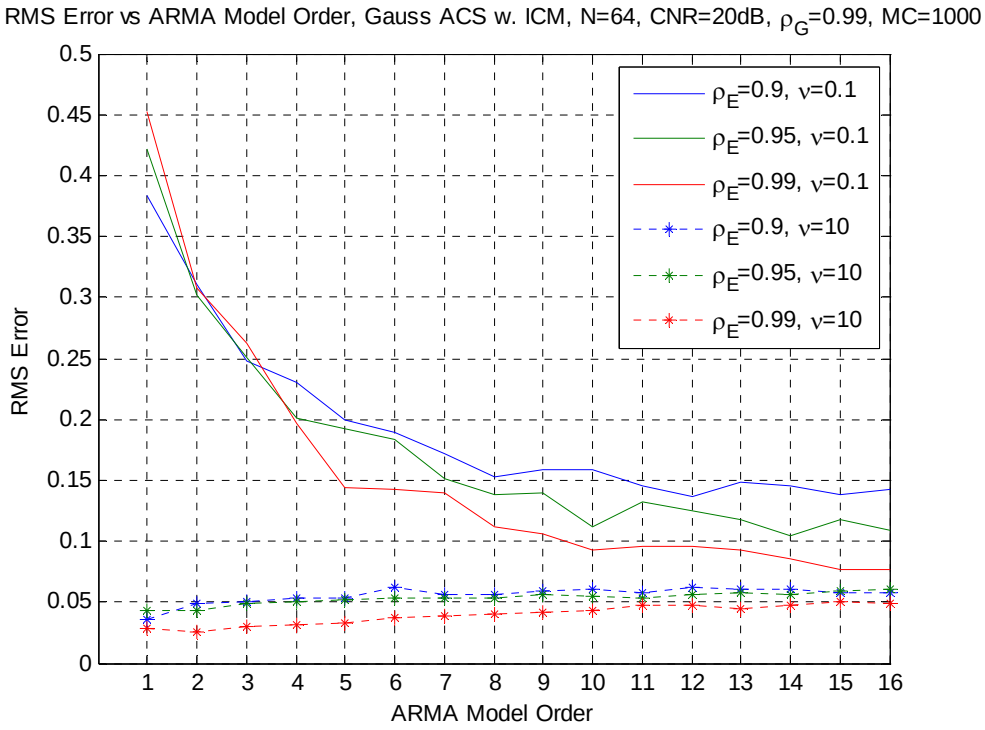

Figure 4-13: ARMA Spectral Estimator Performance for Different Correlation Coefficients at Clutter Shape Parameters (ν) 0.1 and 10

From above results, as in the case of exponential ACS structure, we observe that the ARMA modeling performance is improved with increasing the correlation coefficient, ρ_E. This is an expected result since as the correlation among signal samples increases, the estimation performance increases.

From simulation results, we observe that the ARMA spectral estimator performs differently under different models for the clutter covariance. In fact, unless there is prior information regarding the environmental conditions and radar parameters, such as 3-dB beam-width and PRF, one cannot determine the type of covariance matrix. Moreover, the clutter shape parameter cannot be known in advance. Therefore, in this thesis, a suitable ARMA model order is chosen for comparison purposes. From the simulation results, we selected ARMA(5,5) model as it gives desirable results for spiky (i.e., small shape

parameter) K-distributed clutter without degrading the performance significantly for the Gaussian case.

CHAPTER 5

PERFORMANCE COMPARISON

5.1. Method of Comparison

In this chapter, the performance of clutter suppression using ARMA spectral estimator, which is called ARMA-CS, and conventional methods (such as MTI processor with coherent integrator and optimum filter) are compared. For this purpose, we simulate a set of N coherent radar pulses consisting of a target signal, clutter signal and thermal noise, with predefined signal powers. The clutter signal is suppressed using the techniques mentioned above.

First, we obtain the filters described by N complex weights $(w_1, w_2, \ldots)$ for each technique. The filters used in the comparison are:

- MTI filter cascaded with coherent integrator
- The optimum filter (in the expected mean squared error (MSE) sense) obtained from known interference covariance matrix
- ARMA-CS filter obtained from ARMA spectral estimation method applied to N returned pulses consisting of target, clutter and noise signal

- SMI (Sample Matrix Inversion) filter obtained from estimated covariance matrix that is obtained by standard biased ACS method given in equation (3.9) applied on N pulse returns

The details regarding the determination of filter coefficients are given in the next section. In this section, we define the figure of merit used to assess the clutter rejection performance of these filters are.

The method of comparison is the improvement factor (IF) that is commonly used to describe the performance of linear filters in suppressing clutter. IF is defined as follows [17]:

$$IF = \frac{(SCNR)_O}{(SCNR)_I}. \tag{5.1}$$

where $(SCNR)_I$ and $(SCNR)_O$ denote the signal to clutter plus noise (interference) power ratio at the input and at the output of the linear filter, respectively.

In order to determine $(SCNR)_I$, the clutter plus noise and target signal powers are required. That is, let P_T, P_C and P_N denote the target, clutter and thermal noise powers, the $(SCNR)_I$ can be determined from equation (5.2), [17].

$$(SCNR)_I = \frac{P_T}{P_C + P_N}. \tag{5.2}$$

The expression for $(SCNR)_O$ is as follows [17]:

$$(SCNR)_O = \frac{w^H E\{\bar{s}\bar{s}^H\} w}{w^H M w}. \tag{5.3}$$

Here, w is the transversal filter coefficients, $\bar{s}$ is the $Nx1$ complex target signal vector which is accepted as Swerling-0 (Marcum) in the simulations, M is NxN interference (clutter plus noise) covariance matrix. Moreover, in (5.3) $(\cdot)^H$ indicates Hermitian (transpose conjugate) operation, and $E\{\cdot\}$ denotes statistical average operation.

In fact, the target return for the i[th] pulse can be determined as follows:

$$s_i = \sqrt{P_T}\exp(-j2\pi(i-1)f_D) \qquad i = 1,2,...,N. \tag{5.4}$$

where f_D denotes the normalized target Doppler frequency, which is obtained by dividing the target Doppler frequency with PRF. The interference covariance matrix is:

$$M = \frac{P_C}{P_N} R_C + I. \tag{5.5}$$

where P_C and P_N denotes the input power of clutter and noise, respectively. Here, R_C is NxN clutter covariance matrix and I is the identity matrix to represent white Gaussian thermal noise covariance matrix.

5.2. Transversal Filter Coefficients for Processors

As seen from equation (5.3), the transversal filter coefficients, w, are required to determine $(SCNR)_O$ for each processors. In what follows we describe the

methods to determine the transversal filter coefficients for processors are given.

- **MTI and Coherent Integrator Processor (CI)**

In this processor, the weights of transversal filter, w, are evaluated by cascading an MTI filter and a coherent integrator (CI). Let us denote the MTI filter coefficients by w_{MTI} and coherent integrator weights by w_{CI}. The transversal filter weights are determined from equation (5.6)

$$w = w_{MTI} \otimes w_{CI} . \tag{5.6}$$

where $\otimes$ denotes convolution operation. In the simulations, for MTI filter double delay line canceller is considered. Furthermore, since the target Doppler frequency is assumed to be known, the coherent integrator is set to that frequency.

For convolution operation the resulting filter has a number N samples equal to:

$$N = N_{MTI} + N_{CI} - 1. \tag{5.7}$$

where N_{MTI} and N_{CI} are samples of corresponding filters. The weights w_{MTI} and w_{CI} are given as:

$$w_{MTI} = (1,-2,1). \tag{5.8}$$

$$w_{CI} = \exp(-j2\pi f_D (i-1)) \qquad i = 0,1,...,N-2 . \tag{5.9}$$

- **Optimum Processor**

The clutter is characterized well as K-distributed random processes [1]; therefore, conventional filtering approaches, such as MTI and coherent integration, are not utilized as optimum processing [18]. However, with the optimum filter for Gaussian interference approach [17] and GLRT detector for perfectly known signal (Swerling-0) approach [18], an optimum processor can be designed in the mean squared error sense.

The optimum transversal filter weights for a target with known Doppler velocity, which is the case in our simulations, is given by:

$$w = M^{-1}\bar{s}^{*}. \tag{5.10}$$

where M^{-1} is the inverse of the interference (clutter plus noise) covariance matrix.

- **ARMA-CS Processor**

The ARMA-CS processor uses the ARMA spectral estimation method to determine the transversal filter coefficients for a certain ARMA model order. To estimate the transversal filter coefficients, the ARMA method is applied on the interference signal where no target signal exists. That is, to estimate the ARMA-CS transversal filter coefficients, we assume that there is no target present in the range cell under consideration.

Using the ARMA spectral estimation method, the power spectral density (PSD) of the interference (clutter plus noise) signal is initially estimated for predetermined ARMA pole and zero orders (in our case, pole and zero orders are 5). That is, $A(f)$ and $B(f)$, which are the polynomials with predetermined orders, must be determined from ARMA method. The structure of $A(f)$ and $B(f)$ are shown in equation (5.11).

$$\begin{aligned} A(f) &= 1 + a_1 e^{-j2\pi f} + a_2 e^{-j4\pi f} + \ldots + a_n e^{-jn2\pi f} \\ B(f) &= 1 + b_1 e^{-j2\pi f} + b_2 e^{-j4\pi f} + \ldots + b_m e^{-jm2\pi f} \end{aligned}. \tag{5.11}$$

Using (5.11), the PSD of the interference (clutter plus noise) signal is obtained.

$$\phi_{ARMA}(f) = \sigma^2 \left| \frac{B(f)}{A(f)} \right|^2 \qquad -1/2 \le f \le 1/2. \tag{5.12}$$

The inverse FFT of the PSD yields the ACS, i.e., the first row of the ARMA covariance matrix so that the following Fourier transform relationship is valid.

$$r_{ARMA}(k) \overset{FFT}{\leftrightarrow} \phi_{ARMA} \tag{5.13}$$

The covariance matrix of ARMA process, R_{ARMA}, can easily be obtained from the r_{ARMA} vector.

$$R_{ARMA} = \begin{bmatrix} r_{ARMA}(0) & r^*_{ARMA}(1) & \cdots & r^*_{ARMA}(N-1) \\ r_{ARMA}(1) & r_{ARMA}(0) & \ddots & \vdots \\ \vdots & \ddots & \ddots & r^*_{ARMA}(1) \\ r_{ARMA}(N-1) & \cdots & r_{ARMA}(1) & r_{ARMA}(0) \end{bmatrix}. \tag{5.14}$$

Finally, the ARMA-CS processor transversal filter coefficients can be obtained as follows:

$$w = R^{-1}_{ARMA} \bar{s}^*. \tag{5.15}$$

- **SMI (Sample Matrix Inversion) Processor**

In the two preceding sub-sections, the covariance matrix of interference is used exactly and estimated via ARMA spectral estimation method. In this type of processor, which is called as SMI processor, the interference covariance matrix is estimated using the interference data directly. That is, for estimation purposes, it is assumed that the range bin does not contain any target signal. It only contains the interference signals, clutter and noise.

First, the ACS is estimated using equation (3.9):

$$\hat{r}_{SMI}(k) = \frac{1}{N}\sum_{t=k+1}^{N} x(t)x^{*}(t-k) \qquad 0 \le k \le N-1. \tag{5.16}$$

The corresponding covariance matrix, R_{SMI}, can easily be obtained from $\hat{r}_{SMI}$ vector.

$$R_{SMI} = \begin{bmatrix} \hat{r}_{SMI}(0) & \hat{r}^{*}_{SMI}(1) & \cdots & \hat{r}^{*}_{SMI}(N-1) \\ \hat{r}_{SMI}(1) & \hat{r}_{SMI}(0) & \ddots & \vdots \\ \vdots & \ddots & \ddots & \hat{r}^{*}_{SMI}(1) \\ \hat{r}_{SMI}(N-1) & \cdots & \hat{r}_{SMI}(1) & \hat{r}_{SMI}(0) \end{bmatrix}. \tag{5.17}$$

Finally, the SMI processor transversal filter coefficients can be obtained with the optimum filter approach in the mean square error sense.

$$w = R^{-1}_{SMI}\bar{s}^{*}. \tag{5.18}$$

5.3. Results

For comparison, we evaluate the improvement factor (IF) for each processor under varying conditions. The assumptions regarding the simulation setting are as follows:

i. In a dwell time, the PRF remains constant; i.e. the pulse train is uniformly spaced in time.

ii. The target Doppler frequency is known and does not change during the dwell time.

iii. For ARMA-CS processor and SMI processor, Monte Carlo simulations are carried out to estimate the corresponding IF. In the simulations, the number of Monte Carlo runs is 500.

iv. The coherent integrator is tuned to the target Doppler frequency. Moreover, the shaping losses observed in practical radars are neglected.

v. The transversal filter length N is the same for all processors.

vi. The radar parameters, such as PRF, antenna beam-width and angular rotation speed, remain the same in the simulations except for the number of processed pulses.

vii. The exponential correlation factor, ρ_E, determining the covariance matrix varies between simulations except for the Gaussian case, for which it depends on the constant radar parameters.

As seen in Chapter 4, the modeling performance of the ARMA spectral estimator depends on the shape parameter of the K-distribution. This is also the case for the SMI processor that uses the interference signal to estimate the clutter covariance matrix. However, the performance of the MTI plus coherent integrator processor and that of the optimum processor do not depend on the

shape parameter for the calculation of the IF. Therefore, in order to see the effect of the shape parameter on the IF obtained by the ARMA-CS processor and the SMI processor, two shape parameters, 0.1 and 10, are used to have K-distributed and Gaussian clutter signals, respectively. For both conditions, we assume there is no prior information regarding the environmental conditions, and the ARMA model order is taken as (5,5).

In determination of the IF values, we observe that the signal power is not relevant since it is cancelled in taking the ratio of input and output powers. However, it is obvious that the IF values changes with respect to varying number of pulses, CNR values and target Doppler frequencies. Therefore, the IF values are obtained accordingly for all types of clutter covariance matrices.

The IF figures obtained by processors are shown below for different clutter covariance matrices with respect to the number of pulses. In all of the simulations, the CNR is taken as 25 dB, the normalized target Doppler frequency is 0.2, which is outside the region where the most of the clutter power is contained in the PSD.

In Figure 5-1, the IF of processors for different shape parameters is illustrated for covariance matrix which has Gaussian ACS structure.

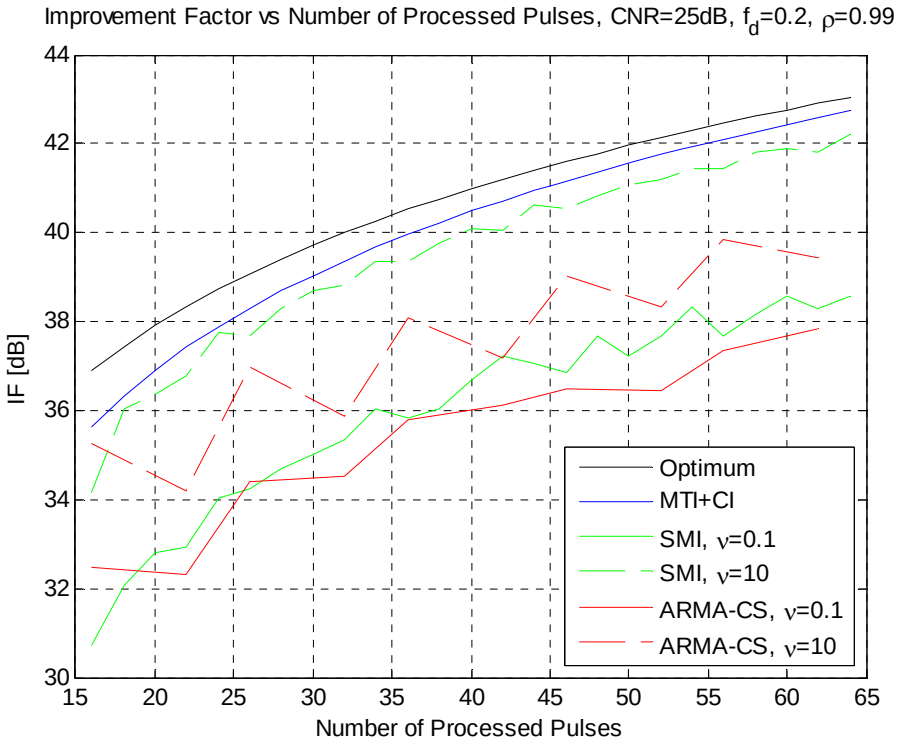

Figure 5-1: Improvement Factor of Processors versus the number of processed pulses for Gaussian ACS.

For Gaussian clutter covariance matrix, we observe that the MTI plus coherent integrator performs slightly worse (about 1 dB) compared with the optimum processor. For the ARMA-CS and SMI processors, when the clutter shape parameter is small, the IF figures are small because of the degradation in the estimation performance of the biased ACS, as explained in Chapter 4. For higher values of the shape parameter, IF values are higher, but still smaller than that of MTI plus coherent integrator. However, except for the cases with smaller number of pulses, ARMA-CS processor is worse than the SMI processor due to the computational errors in the estimation of ARMA parameters. For small number of pulses, IF values obtained from the ARMA-CS processor is better than that of the SMI processor and close to that of MTI

plus coherent integrator due to less significant errors made in determining the ARMA parameters.

For covariance matrix generated from exponentially decaying correlation coefficient resulting from internal clutter motion (ICM), the IF values of different processors versus number of processed pulses are shown in Figure 5-2, where the simulation parameters are the same as in the Gaussian case. In addition, the correlation factor of exponential ACS is taken as 0.99, which corresponds to a wind velocity of 9.65 mph for a radar with 10 GHz carrier frequency.

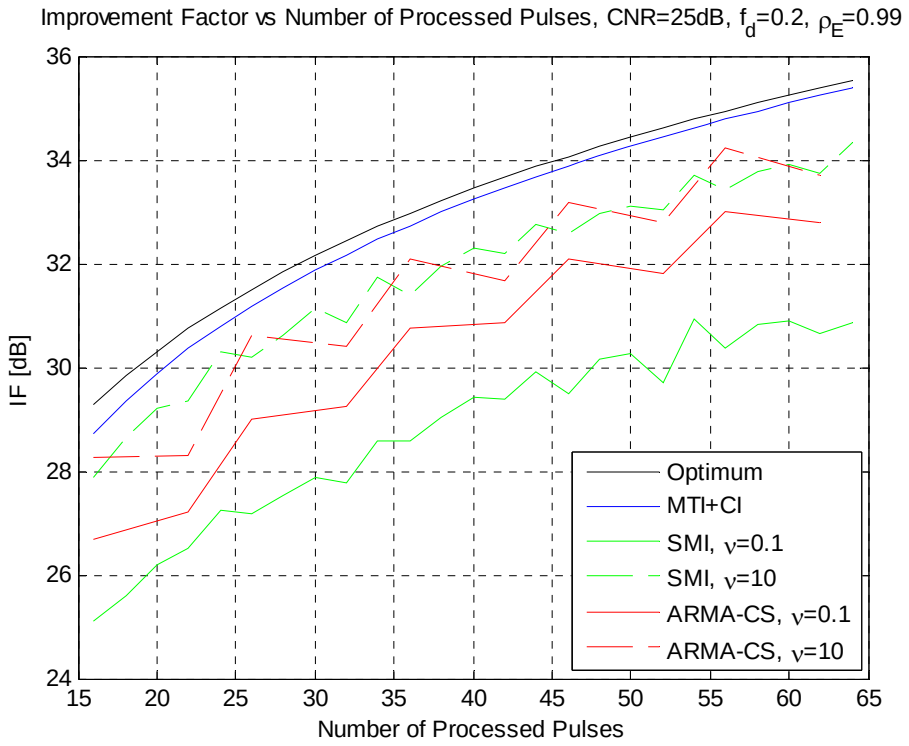

Figure 5-2: Improvement Factor of Processors versus the number of processed pulses for Exponential ACS.

From Figure 5-2, it is seen that the SMI processor gives poor results for spiky clutter since the biased ACS performs worse for K-distributed interference signals. However, the ARMA-CS processor results in higher IF values for spiky clutter. For the Gaussian distributed clutter, both SMI and ARMA-CS processor performances are better. The MTI plus coherent integrator is very close to optimum processor and still performs better than both processors.

The IF figures are also obtained for Gaussian clutter covariance matrix tapered with ICM in Figure 5-3. The results are illustrated for the same radar parameters, normalized frequency, and CNR. The correlation factor for ICM is taken as 0.99.

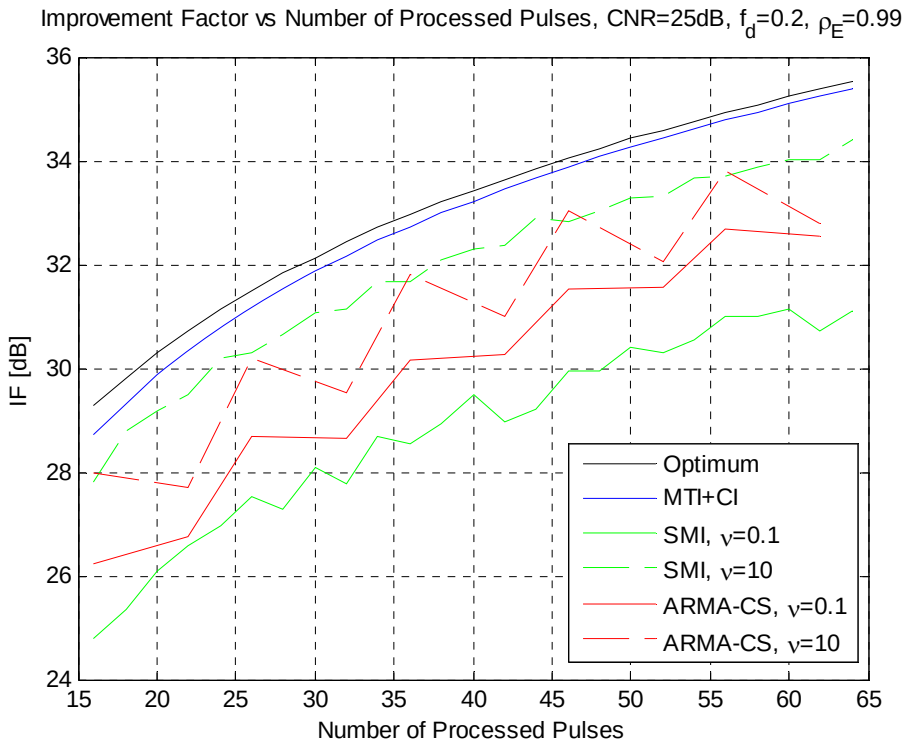

Figure 5-3: Improvement Factor of Processors versus the number of processed pulses for Gaussian ACS tapered ICM.

The results are nearly the same as the exponential clutter covariance, except that the SMI processor performs slightly better due to the effect of Gaussian covariance matrix caused by antenna scanning modulation. However, for all of the clutter covariance types, it is seen that for small number of processed pulses, ARMA-CS performs better than SMI processor but worse than MTI plus coherent integrator.

The IF values of processors are evaluated for different clutter covariance structures as a function of CNR values. In the simulations, in order to satisfy spectral distance between clutter and target, target normalized frequency is again taken as 0.2. Moreover, the correlation factors which are caused by antenna scanning modulation for Gaussian clutter and internal clutter motion for exponential clutter are the same as in previous simulations. Finally, the number of pulses is taken as 32 in the simulations.

The IF values of processors for clutter covariance matrix from Gaussian ACS are shown in Figure 5-4.

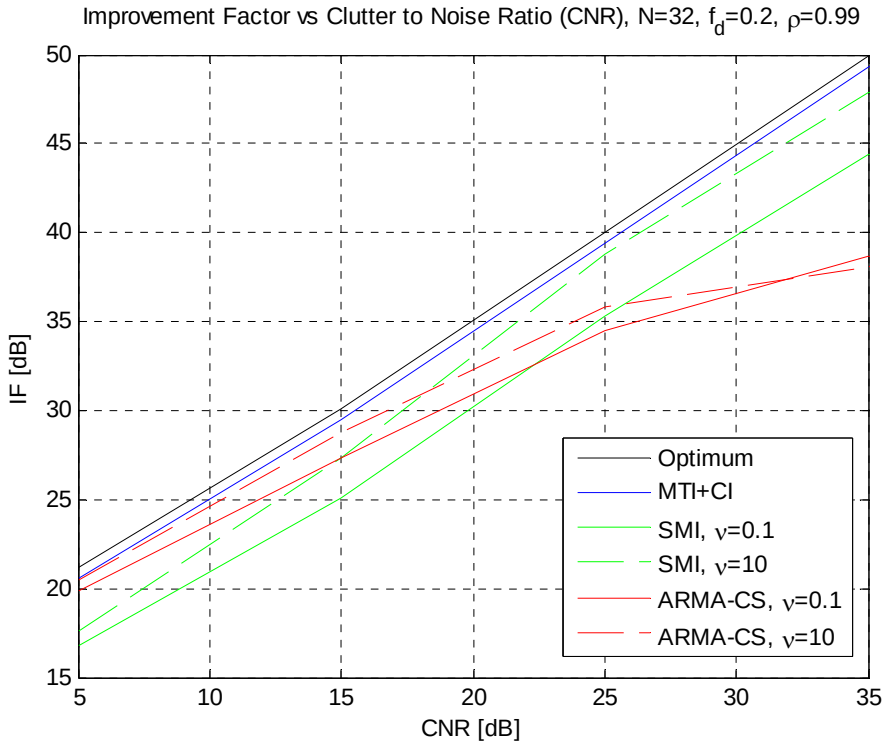

Figure 5-4: Improvement Factor of Processors versus CNR for Gaussian ACS.

We observe that, due to the poor estimation of ACS in SMI and ARMA-CS processors, the IF figures are less than those of Gaussian clutter signal (with a larger shape parameter). For all of the CNR values, MTI plus coherent integrator has nearly the same IF values obtained by the optimum processor. However, it is well observed that for low CNR values, the ARMA-CS processor and MTI plus coherent integrator has the same performance. But with increasing CNR, we always expect to see an increase performance of ARMA-CS processor because the information extracted from clutter signal increases. For small CNR values, the ARMA-CS processor performance increases with increasing CNR as expected. However, for high CNR values, the performance improvement in ARMA-CS processor degrades due to the computational errors and use of less data in computation of higher ARMA orders. Since these kinds of computational problems are not seen in other processors, their performances improve with increasing CNR.

We conducted the same simulations for exponential and Gaussian ACS tapered with ICM structures. In addition to the parameters used for Gaussian covariance matrix simulations, the correlation factor due to ICM is taken as 0.99. The exponential clutter covariance matrix simulation results are shown in Figure 5-5.

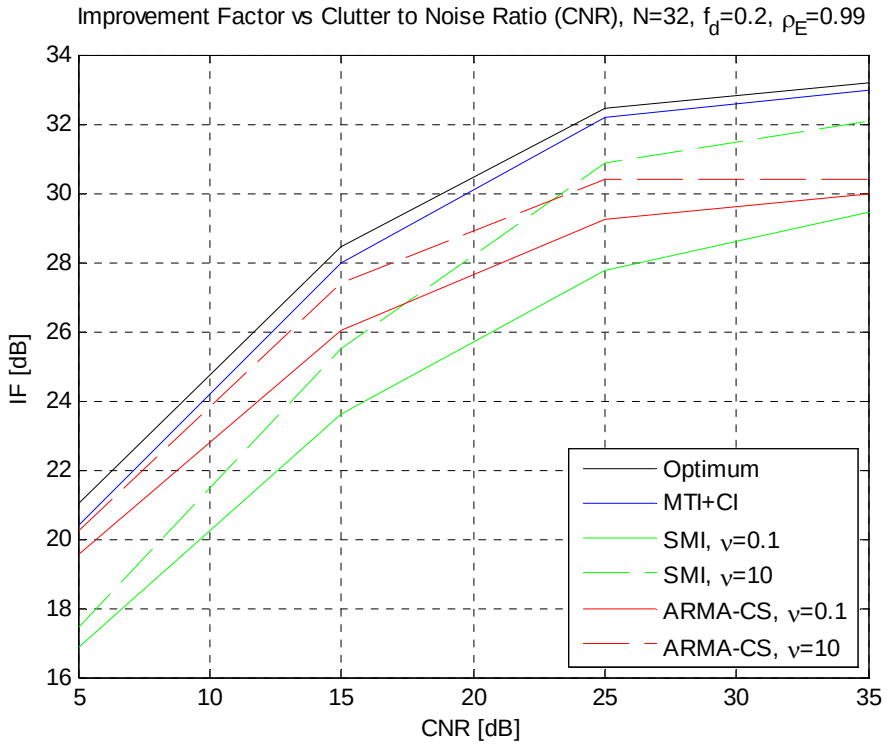

Figure 5-5: Improvement Factor of Processors versus CNR for Exponential ACS.

For all of the processors considered, we do not see a linear increase with respect to CNR that is observed for Gaussian ACS structure for different CNR values. Nevertheless, the general behavior is the same except that the SMI processor IF values are smaller than those of the ARMA-CS processor for spiky clutter with exponential ACS structures. Again for small CNR values,

ARMA-CS processor has nearly the same IF values obtained for MTI plus coherent integrator.

The simulation results for Gaussian covariance matrix tapered with ICM are shown Figure 5-6. In this case, the simulation parameters are the same as those used for the case with exponential ACS structure.

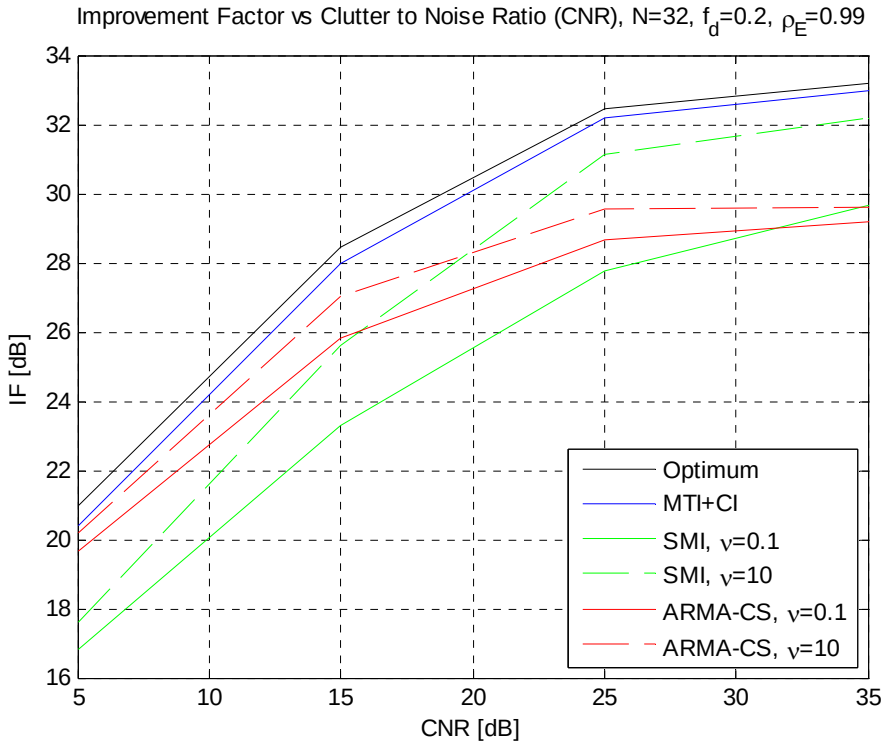

Figure 5-6: Improvement Factor of Processors versus CNR for Gaussian clutter ACS tapered with ICM.

The results obtained in clutter with Gaussian covariance matrix tapered with ICM have the same behavior observed in exponential clutter covariance case. However, we see that due to Gaussian covariance matrix caused by antenna scanning modulation, the IF figures decrease for ARMA-CS and SMI

processors with respect to exponential clutter covariance matrix caused by ICM alone.

From all of the above results, we can conclude that for small CNR values (less than 5dB), ARMA-CS processor gives at least the same performance obtained in MTI plus coherent integrator.

In order to examine the effect of the spectral distance between target and clutter, the IF figures of processors are obtained for various normalized target Doppler frequencies. The number of pulses is taken as 32 and CNR value is set to 25 dB in the simulations. Moreover, the correlation coefficient due to antenna scanning modulation is obtained using the same radar parameters and the correlation coefficient resulting from internal clutter motion (ICM) is taken as 0.99.

The IF figures of processors with respect to normalized target Doppler frequencies are illustrated for Gaussian ACS in Figure 5-7.

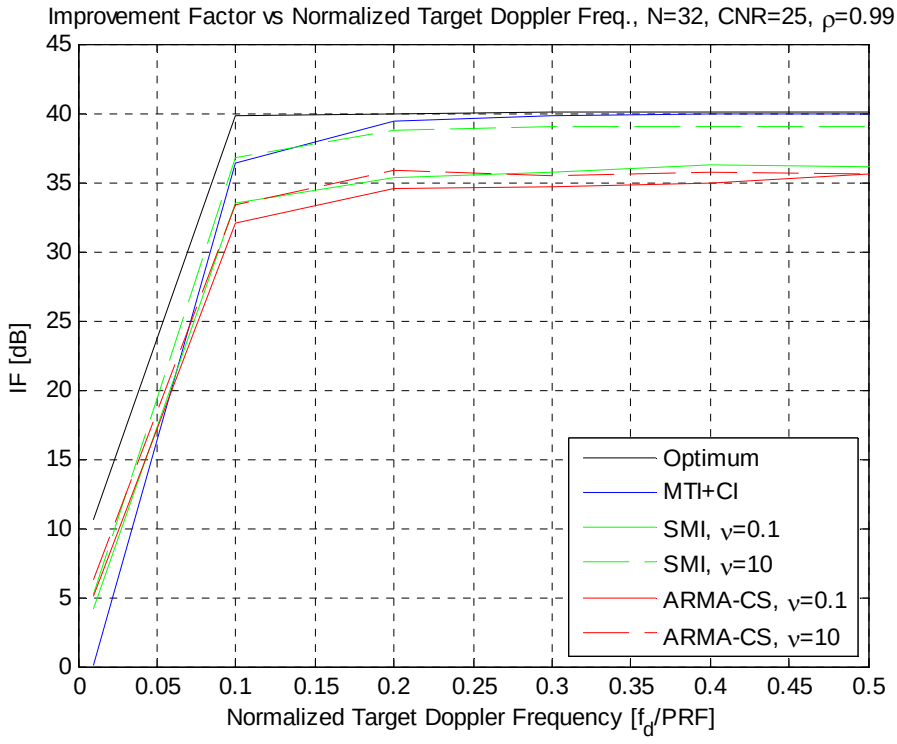

Figure 5-7: Improvement Factor of Processors versus Normalized Signal Doppler Frequency for Gaussian ACS.

From Figure 5-7, we observe that for low target Doppler frequencies in which the spectral separation of clutter and target are weak, the ARMA-CS processor performs better than the MTI plus coherent integrator since the MTI filters the target signal along with the clutter at low Doppler frequencies. In addition, except for higher Doppler frequencies, the ARMA-CS processor and the SMI processor have nearly the same IF values.

As the normalized target Doppler frequency increases, MTI plus coherent integrator has nearly the same IF value as that of the optimum processor. For the ARMA-CS processor and SMI processor, the IF figures obtained for spiky clutter and Gaussian distributed clutter coincide with the previous simulation results.

For exponential ACS structure obtained from ICM, we performed the same simulations with a correlation factor of 0.99. The results are shown in Figure 5-8.

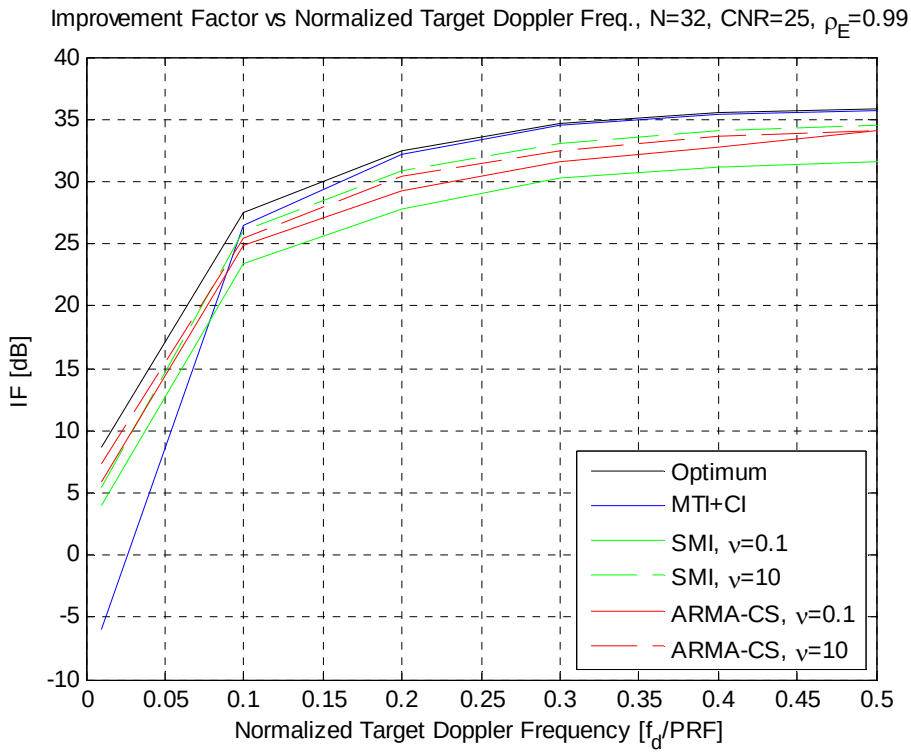

Figure 5-8: Improvement Factor of Processors versus Normalized Signal Doppler Frequency for Exponential ACS.

For exponential ACS structure, the performance of the ARMA-CS processor is better than the Gaussian case. Moreover, ARMA-CS processor gives better IF values compared with MTI plus coherent integrator for lower target Doppler frequencies. Since the clutter PSD actually stems from an exponential ACS structure, the ARMA-CS processor also has a better performance; similar to the case where the SMI processor has better performance for Gaussian signals.

For higher target Doppler frequencies, MTI plus coherent integrator converge to the optimum processor. For the ARMA-CS and the SMI processors, the results coincide with the previous results obtained with different clutter ACS structures, such as Gaussian and exponential.

For Gaussian ACS structure resulting from antenna scanning modulation tapered with internal clutter motion (ICM), the effect of spectral separation of target and clutter is illustrated in Figure 5-9, for the same radar and clutter parameters used to generate antenna scanning modulation and ICM.

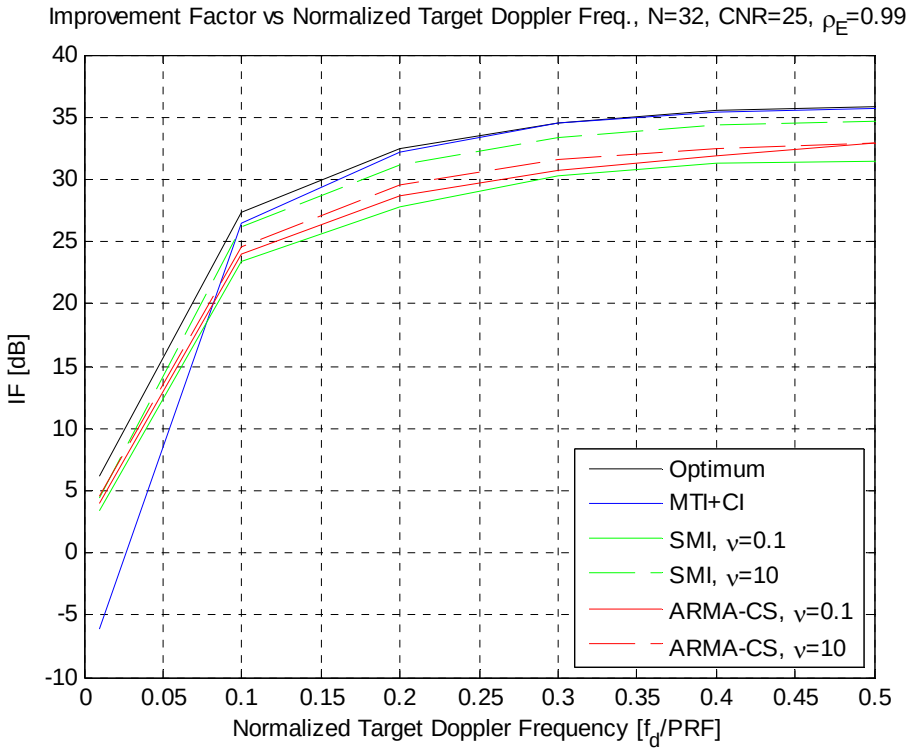

Figure 5-9: Improvement Factor of Processors versus Normalized Signal Doppler Frequency for Gaussian ACS tapered with ICM.

Obviously, when the Gaussian clutter covariance matrix is tapered with ICM, the performance behavior of the techniques is similar to that of the exponential ACS structure resulting from ICM alone. However, the ARMA-CS and SMI processor IF figures are degraded with respect to Gaussian ACS structure case.

Finally, some simulations are performed in order to see the effect of correlation coefficient on IF figures with respect to number of processed pulses. In the simulations, the exponential ACS is used since exponential ACS is mainly caused by the environmental conditions and the desired correlation coefficient can easily be chosen.

The IF figures obtained for different processors are investigated for correlation coefficients equal to 0.7 and 0.5, corresponding to wind velocities of 12.1 mph and 15.0 mph for a radar with 10 GHz carrier frequencies. Moreover, in all of the cases, the number CNR is taken as 25 dB and normalized target Doppler frequency is taken as 0.2. Furthermore, the simulations are performed clutter shape

In Figure 5-10, the IF figures with respect to number of processed pulses for exponential ACS with correlation factor equals to 0.7 are illustrated.

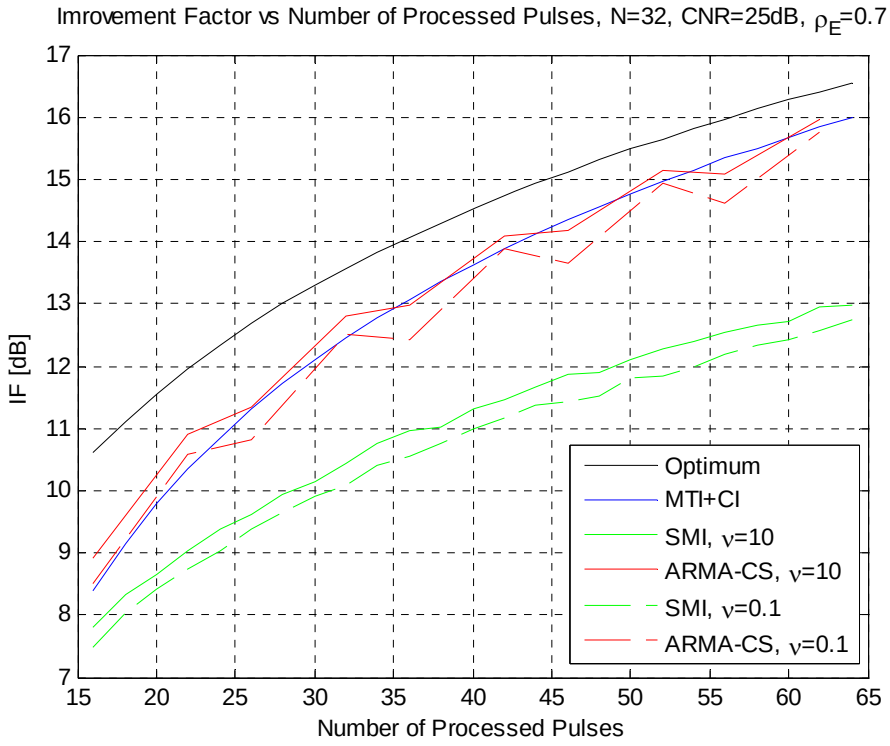

Figure 5-10: Improvement Factor of Processors versus Number of Processed Pulses for Exponential ACS with $\rho_E = 0.7$.

In Figure 5-11, the IF figures with respect to number of processed pulses for exponential ACS with correlation factor equals to 0.5 is shown.

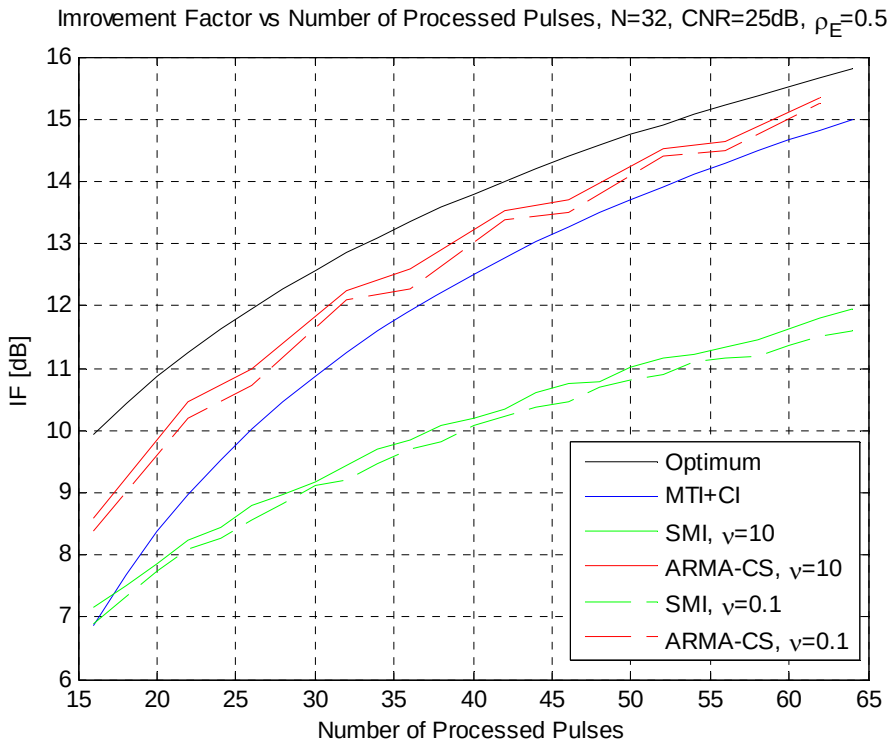

Figure 5-11: Improvement Factor of Processors versus Number of Processed Pulses for Exponential ACS with $\rho_E = 0.5$.

From the previous two results, we see that as the correlation among clutter samples decreases, the ARMA-CS processor gives better IF values compared with MTI plus coherent integrator. This is because MTI plus coherent integrator filter performs better for highly correlated radar pulses. As the correlation among received radar pulses decreases, the performance of all processors decrease but IF figures obtained from MTI plus coherent integrator deteriorate more than ARMA-CS processor. Moreover, since the correlation among samples decreases, the SMI processor gives the worst IF values.

From these results, we can conclude that the ARMA-CS processor performs better than MTI plus coherent integrator in two cases. The first case is when the target signal and clutter signal are in the same Doppler frequency band, i.e.,

when the spectral separation of clutter and target is low. However, compared with the SMI processor, the performance depends on the ACS structure (type of covariance matrix) of the clutter for lower target Doppler frequencies. The second case is when the correlation among clutter samples decreases; i.e., the correlation coefficient of clutter decreases, the ARMA-CS processor gives better IF values than MTI plus coherent integrator processor. For the SMI processor, as the correlation among clutter samples decreases, the IF values obtained become the worst results among the IF values obtained from the other processors

CHAPTER 6

CONCLUSION

6.1. Summary

The main objective of the thesis was investigating the performance of ARMA-CS, using ARMA spectral estimation method, in K-distributed clutter suppression for various clutter shape parameters and ACS structures.

For this purpose, clutter which is generated according to SIRV approach having K-distribution and clutter covariance matrix structures are introduced. After giving information about the target and noise models, the basic spectral estimation concepts are discussed by giving the non-parametric and parametric spectral estimation techniques.

In order to determine the ARMA model order effect on estimation of clutter, RMS errors are calculated for different clutter shape parameters and clutter ACS structures. From the results, it is observed that the RMS error has same type of behavior for different clutter ACS structures. However, for different shape parameters, the behaviors of RMS errors change. In fact, for a spiky clutter (where shape parameter is small), RMS error was decreasing with increasing model order. For clutter whose distribution is approximated by

Gaussian distribution (where shape parameter is large), RMS error increases with in increasing model order, due to computational errors. Accordingly, a suitable ARMA model order has been selected with no a priori knowledge about clutter shape parameter.

The clutter suppression of ARMA-CS with selected ARMA model order is compared with conventional estimators, such as MTI plus coherent integrator. Improvement factor (IF) is used as a performance measure. For this purpose, the transversal filter coefficients for ARMA-CS and conventional methods are determined. The transversal filter coefficients of processors then applied on IF equation consisting of target signal model for comparison. From the results it was observed that the ARMA-CS gives better results for K-distributed clutter approximated as Gaussian distributed signal (large shape parameter). However, ARMA-CS does not give much benefit compared with MTI plus coherent integrator when the spectral separation of clutter and target signal or number of processed pulses is large. Nonetheless, when the spectral separation of clutter and target signals or correlation among clutter samples are small, the ARMA-CS gave sufficient IF values compared with conventional methods.

6.2. Future Work

There are some topics regarding clutter suppression subject to further developed with parametric methods. These topics are as follows:

i. The clutter distribution can be changed to see the performance of ARMA-CS method.

ii. Different spectral estimation methods, such as non-parametric Welch method or parametric AR clutter suppressor utilizing AR technique, may be compared with conventional clutter suppression methods.

iii. In calculation of parameters of parametric spectral estimator, biased ACF equation which is optimized for Gaussian signals is used. For

other types of distributions, such as K-distributed or Weibull distributed, the ACS of clutter signals can be estimated with equations optimized for those distribution types.

iv. Clutter shape parameter and ACS structure may be estimated from the clutter data prior to clutter suppression to find the optimum model orders of ARMA spectral estimator.

v. The ACS of clutter caused by ICM is accepted as exponential. However, other models which cannot be modeled by an exact parametric model exist in literature [1]. Those models of ICM may be used to see the performance change of processors.

REFERENCES

[1] Richards,M.A., Fundamentals of Radar Signal Processing,1st Ed. McGraw-Hill, New York, 2005.

[2] Antipov I., "Simulation of Sea Clutter Returns", Tactical Surveillance System Division, Elecytonic and Surveillance Research Laboratory, DSTO-TR-0679, June 1998.

[3] Totir F., Rador E., Anton L., Ioana C., Şerbanescu A., Stankovic S., "Advanced Sea Clutter Models and Their Usefulness for Target Detection", MTA Review, Vol. XVIII, No.3, Sep. 2008.

[4] Ward K.D., "Compound Representation of High Resolution Sea Clutter", Electron. Lett., Vol. 17, pp. 561-563, 1981.

[5] Ward K.D., "A Radar Sea Clutter Model and Its Application to Performance Assesment", IEE Conf. Publ. 216, Radar-82, pp. 203-207, 1982.

[6] Ryan, J. and Johnson, M., "Radar Performance Prediction for Target Detection at Sea", IEE Conf. Proc. No 365, Radar-92, pp. 13-17, 1992.

[7] Baker, C.J., "K-Distributed Coherent Sea Clutter", IEE Proc., Vol. 138, Pt. F, No 2, pp. 89-92, April 1991.

[8] Chan, H.C., "Radar Sea Clutter at Low Grazing Angles", IEE Proc., Vol. 137, Pt. F, No 2, pp. 102-112, April 1990.

[9] Conte, E., Longo, M., and Lops, M., “Modeling and Simulation of Radar Clutter as a Spherically Invariant Random Process”, IEE Proc., Vol. 134, Pt.F, No 2, pp. 121-130, April 1991.

[10] Rangaswamy, M., Weiner, D., Ozturk, A., “Non-Gaussian Random Vector Identification Using Spherically Invariant Random Processes”, IEEE Trans. AES, Vol. 29, No 1, pp. 111-123, January 1993.

[11] Techau P.M., Bergin J.S., Guerci J.R., “Effects of Internal Clutter Motion on STAP in a Heterogeneous Environment”, IEEE Radar Conf, 204-209, 2001.

[12] Lombardo P., Billingsley J.B., “A New Model for the Doppler Spectrum of Windblown Radar Ground Clutter”, IEEE Radar Conf., Waltham, MA, 1999.

[13] Nathanson, F.E., Reilly, J.P., Cohen, M.N., Radar Design Principles: Signal Processing and Environment, 2nd Ed. McGraw-Hill, 1990.

[14] Stoica, P., Moses, R., Introduction to Spectral Analysis, 1st Ed., Prentice-Hall, 1997.

[15] Kay, S.M., Modern Spectral Estimation: Theory & Application, 1st Ed., Prentice-Hall, 1988.

[16] Proakis,J.G., Rader, C.M., Ling, F., Nikias, C.L., Advanded Digital Signal Processing, Macmillian, 1992.

[17] D’addio, E., Farina, A., Studer, F.A., “Performance Comparison of Optimum and Conventional MTI and Doppler Processors”, IEEE Trans. AES, Vol. 20 No. 6, November 1984.

[18] Gini, F., “Sub-optimum coherent radar detection in a mixture of K-distributed and Gaussian clutter,” IEE Proc.-Radar, Sonar Navig., Vol. 144, No.1, February 1997.